SCALE EFFECTS ON THE REMOTE ESTIMATION OF EVAPOTRANSPIRATION

DISSERTATION

Presented to the Graduate Council of

Texas State University-San Marcos

in Partial Fulfillment

of the Requirements

for the Degree

Doctor of PHILOSOPHY

by

Jiao Wang, B.S., M.S.

San Marcos, Texas

May 2012

SCALE EFFECTS ON THE REMOTE ESTIMATION OF EVAPOTRANSPIRATION

Committee Members Approved:

_____

Nathan Allen Currit, Chair

_____

Jennifer Jensen

_____

Mark Alan Fonstad

_____

Kyle E. Murray

Approved:

_____

J. Michael Willoughby
Dean of Graduate College

FAIR USE AND AUTHOR'S PERMISSION STATEMENT

Fair Use

Duplication Permission

ACKNOWLEDGEMENTS

I am grateful and would like to sincerely thank Dr. Nate Currit for his guidance, understanding, patience, and most importantly, his spiritual and financial support during my graduate studies at Texas State University-San Marcos. Every discussion with him was pleasant and encouraging. He is not just a wonderful advisor but he has also impacted me in being a better person. I am very fortunate to have been able to enjoy and benefit from such a relationship with him.

I would also like to thank all of the committee members for their input, valuable discussions and accessibility throughout my research endeavor. Dr. Jensen's encouragement cheered me up a lot when I was tired from working on the dissertation. Dr. Fonstad's strictness with research reminded me to work hard. Dr. Murray was very caring and always asked me for research updates. I wish I could have spoken more with my committee members.

Additionally, I am very grateful for the eddy covariance data provided by Dr. James L. Heilman from Texas A&M University. Many thanks also go to Mr. Ray Kamps for his kindness in showing me around at Freeman Ranch.

Finally, and most importantly, being the first in my family to go to college, I am grateful to my parents for raising me with tremendous love and support. Without their foresight in education since my early childhood, I would not be able to make it this far earning a PhD in the United States.

This manuscript was submitted on March 6, 2012.

TABLE OF CONTENTS

Page

LIST OF TABLES

Table **Page**

LIST OF FIGURES

Figure **Page**

ABSTRACT

SCALE EFFECTS ON THE REMOTE ESTIMATION OF EVAPOTRANSPIRATION

by

Jiao Wang, B.S., M.S.

Texas State University-San Marcos

May 2012

SUPPERVISING PROFESSOR: NATHAN ALLEN CURRIT

Consideration of spatio-temporal scale in geographic research is often mentioned, but scale effects on geographic modeling are poorly understood. The goal of this research is to explore and test the critical role of geographic relationships as they are represented across multiple spatial scales of analysis and to develop a general methodology for studying scaling relationships. Specifically, this dissertation uses remotely sensed data to

investigate scale dependencies of mass and energy fluxes in the hydrologic cycle by developing a methodology to analyze the scaling relationships of evapotranspiration (ET). This research seeks to answer three categories of questions: (1) What effects do different aggregation techniques have on ET estimation as resolution decreases? How does landscape heterogeneity impact the aggregation process? (2) As major inputs to ET models, do the Normalized Difference Vegetation Index (NDVI) and surface temperature have consistent impacts on estimated ET across scales? Which input has a stronger correlation with ET estimation and does that correlation remain across scales of analysis? (3) How does the spatial autocorrelation of ET vary with scale? Does a relationship exist between the variance of spatial autocorrelation and spatial resolution?

Three analyses were performed to answer these research questions, including a comparison of aggregation techniques, an assessment of the primary indicators of ET, and the spatial autocorrelation of ET estimates. First, two aggregation techniques are used to aggregate ET from 30 meters to coarser resolutions. Findings indicate that the two aggregation techniques used produce statistically different ET estimates at resolutions finer than 960m. A pixel-by-pixel comparison of paired ET estimates at each scale reveals that landscape heterogeneity has an important impact on ET estimation accuracy. Most large pixel-by-pixel differences occur in non-vegetated areas and their boundaries with other land cover classes. Second, a correlation analysis was conducted on ET and its primary indicators across scales. Findings indicate that surface temperature is more

correlated to ET than NDVI at resolutions finer than 240m. At resolution coarser than 240m, the correlations of ET with NDVI, surface temperature become inconsistent. When scale changes, the landscape heterogeneity alters the influence of ET drivers. Third, a geostatistical analysis was performed to study the spatial autocorrelation of ET across scales. Range and partial sill were used to study the spatial autocorrelation of ET. Findings indicate that spatial resolution determines the spatial autocorrelation we observe. When the resolution is finer than a threshold, ranges are identifiable. Finer resolution can better present the variance of landscape than coarser resolution. However, the finest resolution may not be the best resolution to reflect the spatial variability. The resolution with highest partial sill should be used to best represent the landscape's spatial variability.

This research provides a way to study the scaling relationship impacted by the heterogeneity of landscape from three aspects, including the aggregating techniques, correlation of phenomenon and its major indicators, and spatial autocorrelation. As a whole, findings in this study improve our understanding of ET modeling and estimation using remotely sensed data. More importantly, this research elucidates general scale considerations that must be assessed prior to geographic modeling because they influence how we represent cause-effect relationships and the modeling of spatial patterns and processes.

CHAPTER I

INTRODUCTION

1.1 Scale Issue

Scale is "the spatial, temporal, quantitative, or analytical dimensions used to measure and study any phenomenon" (Gibson et al. 2000). Scale has been an important element that appears in all kinds of studies in natural and social science. Researchers usually consider the concept of scale in their research: e.g. local, regional, or global scales for a climate change study (e.g. Blunier and Brook 2001); micro or macro scales for an ecological study of microbial communities (e.g. Balser et al. 2006); community, city, state, or national scales for a social scientist's study on migration (e.g. Levitt 1998); and daily, monthly, seasonal, or annual scales for a hydrological study on stream flow (e.g. Hughes 2004). Scale considerations are ubiquitous in scientific studies.

Caution should be taken when studying a phenomenon at any particular scale. There are four major steps to an ordinary research process: (1) identify or define the phenomenon/problem, (2) collect data, (3) build a model, and (4) validate the simulation/results. Whether the results explain the phenomenon depends on many things and one of them is the scale at which patterns and processes are measured and modeled.

Research has shown that, for the same phenomenon, unique patterns may become evident when modeled at different scales.

Scale, then, is a two-fold concept. On one hand is the scale of the phenomenon itself – the scale at which it occurs. On the other hand is the scale at which the phenomenon is studied, including data sampling and model building. The ideal study would allow for a model to reflect and explain the phenomenon. However, in most cases it is either time/space consuming to clone the reality with every single aspect and detail. If the scale of occurrence and the scale of the data and model match, it will be easier for us to identify the phenomenon and its causal factors. If we select disjointed scales, it will be more difficult for us to fully understand the phenomenon or even not be able to see it, not to mention study it. Moreover, usually it is not necessary to create an identical reflection of the natural or social problems. If we treat the scale issue well in both data and modeling parts, we will still be able to have a general understanding about the problem by gathering appropriate data and building a model that includes major factors and their functions (Figure 1.1).

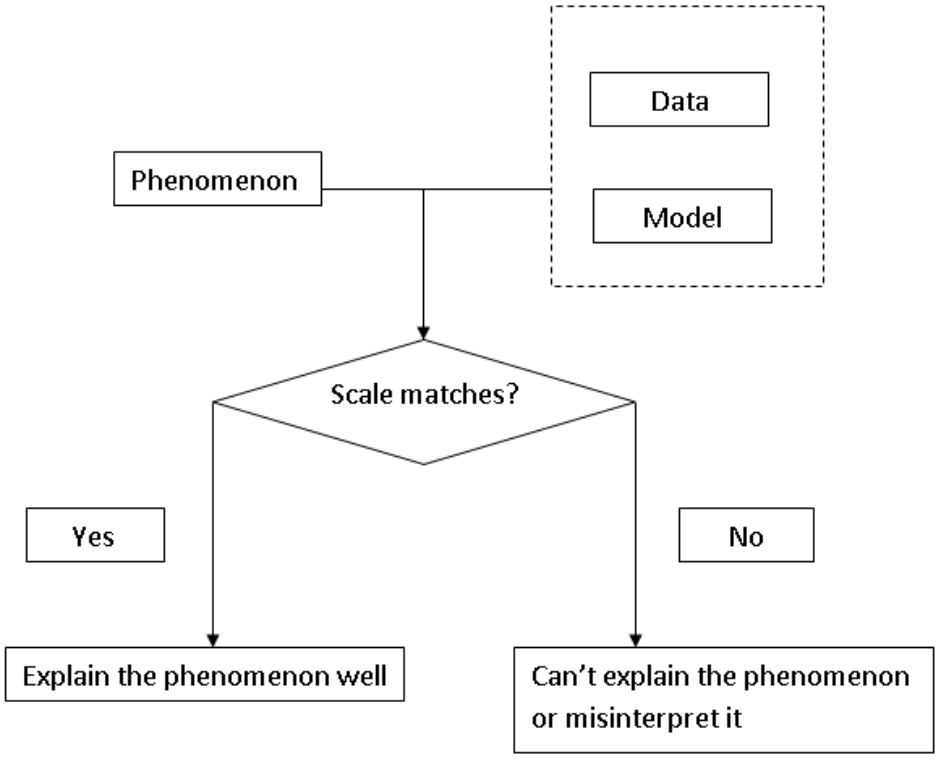

Figure 1.1 The scale at which a phenomenon is represented impacts a model's explanatory power.

One "scale matters" example is the founding event in epidemiology: John Snow located the source of a cholera outbreak near a public water pump in England, in 1854 (Snow 1855). The spatial scale or extent he selected in the search of the source of outbreak played an important role in his effort of detecting the threat to public health. There are two factors in his identification of the source: location and extent. If he had not looked into a study area that included the water pump, but only drew his study area in other neighborhoods, it would not be possible for him to identify the cause of the cholera outbreak. In contrast, if he had selected the water pump neighborhood, but not a large enough surrounding region, he would not have been able to distinguish places with high fatality. His success in identifying the source of the outbreak was due to the successful identification of a scale of analysis. This example shows the importance of spatial scale

or extent for the identification of a phenomenon and its causal factors. Often, however, patterns and processes are embedded within one another which leads to multiple and complex causal relationships. Complex multi-scale systems often exhibit emergent properties, where certain patterns and processes manifest themselves only at certain scales. Moreover, patterns and processes that occur at one scale may change at finer or coarser scales of analysis. This type of change across scales is called a non-linearity (Jarvis 1995). Thus from the spatial perspective of scale, location and size are essential factors to be considered as the beginning step of study.

1.2 Scale Effect

The significance of scale effects has been studied by many scholars (e.g. Bian 1997; Easterling and Polsky 2004; Evans et al. 2003; Gibson et al. 2000; Herod and Wright 2003; Nelson et al. 2007; Walsh et al. 1999; Wu 2004). One aspect of scale effects is scale dependency, which refers to the degree a pattern varies as a function of scale (Wu 2004). For example, when viewed on a global scale (e.g., from Space) the Amazon may appear to be a homogeneous mass of forest. As the viewing distance decreases, however, the heterogeneity of the forest will become apparent. Clusters of trees will become visible; patterns of deforestation and road networks will come into view. At even smaller viewing distances, tree crowns will become apparent and patterns of undergrowth will be visible. In short, the level of homogeneity is dependent on the scale of analysis. Similarly, the ocean may appear to be a homogeneous mass of blue when viewed from Space. Even when viewed at a closer distance, the ocean may still appear to be a mass of blue. Not until decreasing the viewing distance even more will the heterogeneity of the ocean become apparent. The differences in pattern that become

apparent as the scale of analysis changes in the Amazon and ocean examples are due to different patterns of scale dependence. That is, scale dependence is unique to a particular phenomenon. Scale determines what we see and then impacts how we explain what we see.

Scale issues become more complex as scale changes. The magnitude of the impact from some factors might decrease or increase across scales. One factor may have a dominant impact at a particular scale, but weaker at other scales. For example, researchers found that grassland disturbance was from livestock grazing and hay harvest at a large scale and from tracked vehicles at a small scale (Limb et al. 2009).

Turner et al. (1990) pointed out that there are two ways that the local and regional scales relate to global scales. Systemic changes are about fundamental changes in the system triggered by local actions, while cumulative changes are the accumulation of local changes (Wilbanks 2006). These two types of changes indicate that when scale changes the way all factors interact may change as well. We will have to adjust the parameters in the model we create or even have to create a new model if the relationship varies too greatly. Any of these would impact our investigation and understanding of the phenomenon we observe. This is an issue rooted from whether drivers can be passed on unchangeably from one scale to another as in a linear process, and whether the collective working relationship stays the same or not at various scales as in a non-linear process.

1.3 Scale in GIScience

Scale must be a fundamental consideration when geographers describe and explain spatial patterns and processes (Gibson et al. 2000). The traditional geographical

scale (i.e. 1:100,000) represents the map ratio relative to the real world. The paper map has a fixed scale and extent, and provides limited information. The development of geographic information science (GIS) brought paper maps into the digital era, which made it possible for a map to have unlimited scales of display and extent.

Major sources of GIS data are remotely sensed imagery. The spatial resolution is fixed for a particular type of imagery, such as 1km and 500m for MODIS, 30m for LANDSAT 7, and 8m for SPOT 6. These resolutions keep us from studying a phenomenon at finer scales than the resolution, which may result in failure to identify some patterns. On the other hand, we have to aggregate data to study a phenomenon that occurs at a coarser scale than the spatial resolution. Aggregation techniques have to be used, which leads to concerns such as the impacts of aggregation techniques, and how to choose the aggregation technique.

There are issues in the aggregation process when we deal with scales. One example is called the Modifiable Areal Unit Problem (MAUP), first recognized by Gehlke and Biehl in 1934 and later explicitly explained by Openshaw in 1984. Figure 1.2 shows an example of two ways to aggregate four neighboring units: aggregation across rows and aggregation across columns. When data are aggregated, the shape of the aggregated areas has an impact on the resulting values, which leads to different statistical patterns for each aggregation unit. Patterns are not maintained across different levels of aggregation. Census aggregation is a common example of the MAUP. Statistical relationships and spatial patterns vary across block, block group and tract levels of aggregation.

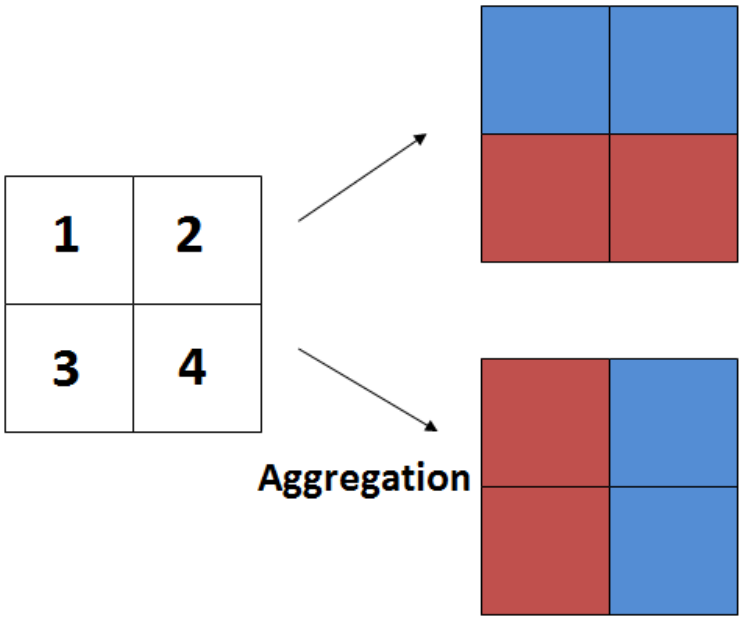

Figure 1.2 Illustration of the modifiable areal unit problem.

It is not possible to go through all scales, thus the chosen scale(s) will need to be appropriate for the research problem. Besides, in many cases, geographers have to use "available scale" for data and models. There may be a scale mismatch between data, models, methods and actual patterns and processes. Multi-scale observation and modeling is helpful or sometimes necessary if we want to fully understand a phenomenon.

1.4 Research Purpose

While many of the patterns we observe in complex systems are scale dependent, the selection of a particular scale to study cause and effect will frequently lead to misinterpretation or an incomplete understanding of a process or pattern. It is, therefore, insufficient to simply search for the single scale that provides the greatest explanatory value, especially when the causal relationship is measured with a coarse indicator of

statistical agreement (i.e. R^2). Instead, we need to analyze how and why the observed process or pattern changes with scale. A thorough understanding of process and pattern in complex systems requires the identification and examination of relationships that derive from cross-scale interactions and scale dependency.

As of yet there is no general theory of scaling relationships, even though there have been a number of studies about scale. The purpose of this research is not to, yet again, find the most appropriate scale for a particular analysis, but instead to examine how causal relationships vary with scale. It is my contention that we discover more about the causal relationship as we understand how cause and effect vary across spatial and temporal scales than we do by merely finding an appropriate scale. Essentially, there is meaning in the pattern of cross-scale variation that must be elucidated in order to fully understand a complex causal relationship. The questions I propose are: Can we develop a means of analyzing scaling relationships that exist in a complex system? What factors do we need to study in the scaling relationship? How do we evaluate roles of factors in the causal relationship? What insight will we gain by an understanding scaling relationships in a complex system?

CHAPTER II

CONCEPTUAL FRAMEWORK

Many environmental change assessments are undertaken at international, national, state and local levels (National Research Council 2007). The significance of multiple, interacting scales within processes of global environmental change has been the focus of many of these studies (McDaniels et al. 2005). A significant component of these studies has been land-use and land-cover change because of its potential to accelerate ecosystem change (Solecki 2001). It is, therefore, important to monitor and model the land surface and vegetation processes at various scales (Verstraeten et al. 2008) when assessing water and carbon dynamics of terrestrial ecosystems. For example, understanding land surface fluxes at various scales is critical for weather and climate modeling (Courault et al. 2005). One of the most important issues related to scale in all sciences is "how scale and resolution affect the identification of patterns" (Gibson et al. 2000). Models developed to monitor land-atmosphere interactions are based on an assumption of homogeneity of the land and atmospheric surfaces. They do not, however, account for variation in vegetation and soil at spatial scales smaller than the grid cell in the model (Bonan et al. 1993). The assumption of homogeneity is rarely met in reality, suggesting that a primary focus of current research should be the exploration of scale and the behaviors of water, carbon and energy fluxes across scales (Brunsell et al. 2008).

2.1 Evapotranspiration and its Measurements

Evaporation, the process by which liquid water changes to water vapor and is transferred to the atmosphere, occurs from many surfaces (e.g. lakes, rivers, oceans, soils and wet vegetation) (Allen et al. 2007). Energy is required to cause evaporation and is normally provided by direct solar radiation. Transpiration is the process by which water from plant tissues is transferred into the atmosphere (Allen et al. 2007). Evapotranspiration (ET) is the collective sum of evaporation and transpiration and is one of the most difficult hydrologic parameters to estimate.

Estimation of regional water cycling requires an understanding of the spatial characteristics of ET and its relationship to Earth surface characteristics (Brunsell et al. 2008). However, not much work has been done to assess how the spatial variability of the Earth surface data (e.g. radiometric temperature and vegetation indices) observed at different scales (i.e. pixel resolutions) translate into spatial variability in modeled fluxes (Brunsell and Gillies 2003). There is a critical need for research to understand the role of landscape heterogeneity and the resulting influence on the scaling behavior of surface fluxes monitored by satellite sensors across scales (McCabe and Wood 2006).

ET estimations can be implemented at various scales ranging from the leaf level to the plant, field and landscape levels (Verstraeten et al. 2008), and using various approaches including the water budget, direct measurement, energy balance and empirical methods (Ahmad et al. 2005). Water budget methods use a hydrologic model to track the water loss in the soil-vegetation system. Direct measurement uses instruments to measure ET at a specific location (e.g. lysimeters, scintillometers, and the eddy

covariance technique). The energy balance method monitors ET via the energy exchange. When using the energy balance method for ET estimation, ET is calculated as a residual of three components including net radiation, soil heat flux and sensible heat flux (Allen et al. 2007).

Eddy covariance flux measurement towers can be used to estimate ET at the plot scale, but have the limitation of only sampling the local environment. Flux towers are not designed to estimate fluxes at large spatial scales where heterogeneity of the fluxes is strong over the land surface and the land and vegetation properties are diverse (Gentine et al. 2007; Santos et al. 2008). Their use is limited to specific sites partly because the operation and maintenance is labor intensive and time consuming (Allen et al. 2007; Gentine et al. 2007). Thus, flux towers are not appropriate for routine measurements at a regional scale. On the other hand, flux tower measurements often provide validation information for models and quantitative information about the physical reality of the environment (Verstraeten et al. 2008).

Remote sensing techniques exist for estimating ET under various topographic and land cover conditions (Price 1990). Remotely sensed data are available at different spatial, temporal and spectral resolutions (Li et al. 2008). Many studies have estimated ET using different sensors, including LANDSAT (Bastiaanssen et al. 2005), ASTER (French et al. 2002), AVHRR (Seguin et al. 1991) and MODIS (Nishida et al. 2003). However, in many circumstances, the spatial resolution of remotely sensed data cannot capture individual features (e.g., buildings, streets, trees), and pixels are comprised of multiple land-cover types (Small 2004). The mixed pixel problem hinders the ability to discriminate individual field conditions that lead to errors in the ET estimation. This

impact is stronger when there is significant sub-pixel variability in land cover, roughness, and soil moisture (Kustas et al. 2004; Moran et al. 1997).

The spatial variation of the surface monitored by remotely sensed data has a large impact on the spatial variation or the modeling and representation of the spatial variation in ET (Kustas et al. 1994). The role of data resolution has been examined by some scholars (Hong et al. 2009; Kustas et al. 2004; McCabe and Wood 2006). Kustas et al. (2004) compared histograms of ET estimations at 60m, 120m, 240m and 960m using a two-source energy balance model to examine if any of these scales can provide enough spatial detail to differentiate ET from individual corn and soybean fields. They recommended a pixel resolution of 250-500m to sample individual fields and discrete land surface types which is partly due to the size of individual fields in the study area (102 by 102 m in dimension). While their research supports this recommendation for an agricultural region with large field sizes (Kustas et al. 2004), 250-500m resolution cannot accurately represent surface heterogeneity when vegetation landscape patterns are smaller than 250m. Li et al. (2008) suggest a pixel resolution on the order of 10m is necessary to discriminate spatial patterns of latent heat flux for a heterogeneous landscape; however, they suggest a 100m pixel resolution still works in areas with large vegetation patches. In reality, the resolution of imagery required to accurately estimate a flux varies by ecosystem type and the spatial arrangement of ecosystem components. It is, therefore, insufficient to merely find the supposed best resolution of imagery for a particular region (higher resolution imagery always provides improved flux estimate results, but is usually too cumbersome for regional analyses, as well as often too expensive and infrequently available). Instead, it is important to understand scaling behavior as the level of data

aggregation (i.e., resolution) increases and decreases. In order to get an accurate estimation of the regional distribution of ET when scale changes, it is crucial to manage scale issues properly between different resolutions (Hong et al. 2009).

Remote sensing techniques are the best tools to quantify "the spatial distribution of vegetation, surface temperature and moisture" (Brunsell et al. 2008). Brown and Rosenberg (1973) first used remotely sensed surface temperature to predict ET for a sugar beet field. More recently, remotely sensed data have been used extensively for ET estimation with various spatial, temporal and spectral resolutions (e.g. Anderson et al. 2007; Bastiaanssen 1998; Carlson et al. 1995; Kustas and Norman 1996; Nishada et al. 2003; Yang et al. 2010). High spatial resolution satellite imagery with a low temporal resolution, like LANDSAT and ASTER imagery have been used to estimate ET at the field scale (French et al. 2002; Moran et al. 1996). However, their repeat cycle is not at a daily frequency (8 days for ASTER, 16 days for Landsat). These methods, therefore, are not well suited for routine ET estimation (Lenz and Baise 2007). AVHRR and MODIS imagery provides more frequent data that can be used for routine ET estimation, but the spatial resolution is between 1 and 5 km (Mecikalski et al. 1999; Seguin et al. 1991). Coarse resolution (e.g., large pixels) data are not suitable for monitoring ET of individual vegetation patches (Kustas et al. 2003).

Remote sensing techniques do not measure surface fluxes directly, instead the techniques measure state variables (e.g. land cover, surface temperature, surface albedo, and emissivity) that have impacts on the fluxes (Tang et al. 2010). Large scale ET estimates, such as simulation models or remote sensing algorithms, often use the relationship between the state variables and fluxes (Bastiaanssen et al. 2005; Santos et al.

2008). Satellite-based remote sensing techniques can be used to monitor a number of sampled fields simultaneously and estimate representative mean ET values for a large area (Tasumi and Allen 2007). Remote sensing data covers large areas inexpensively and efficiently (Allen et al. 2005), and observes the patchiness of landscapes, which is not easy to measure in the field over large areas (McCabe and Wood 2006). Moreover, remote sensing data can provide spatially and temporally explicit information by measuring the reflected or emitted electromagnetic radiation, which allows regular monitoring of ET at regional or continental scales (Gentine et al. 2007; Li and Islam 1999; Sandholt et al. 2002; Verhoef and Bach 2003). By combining multi-spectral information from satellite imagery, different surface variables and parameters (e.g. vegetation fraction, LAI, albedo and emissivity) that are necessary to estimate ET can be extracted (Courault et al. 2005; Sanchez et al. 2008).

There are several surface energy balance models developed to estimate ET at a regional level using satellite imagery, such as the Two-Source Energy Balance Model (Norman et al. 1995), Surface Energy Balance Algorithm for Land (SEBAL) (Bastiaanssen et al. 1998), Surface Energy Balance System (Su 2002), and Mapping Evapo-Transpiration at high Resolution with Internalized Calibration (Allen et al. 2007). Overviews of ET estimation models using remotely sensed data are given by Gowda et al. (2008). Among these models, SEBAL is popular as “an intermediate approach using both empirical relationships and physical parameterizations” (Courault et al. 2005). It is a physically based model that calculates ET as the residual of an energy balance for each pixel of multispectral satellite image. It has been used to estimate energy partitioning at the regional scale using raw satellite data and a minimum amount of in-situ data

(Verstraeten et al. 2008). It requires incoming radiation, the normalized difference vegetation index, surface temperature, and surface albedo and provides parameters for the energy balance fluxes such as sensible heat and soil heat (Bastiaanssen et al. 2005). These parameters can be derived from the visible, near infrared and mid-infrared bands and thermal infrared band from satellite imagery. Actual ET rather than potential ET is calculated in this model (Allen et al. 2005). This model has been evaluated across various areas including the United States, and countries in Africa, Europe and Asia (Bastiaanssen et al. 1998, 2005; Lagouarde et al. 2002; Tasumi et al. 2005). Model error is often reported to be around ±15% for daily ET estimated using SEBAL against ground based measurements (Bastiaanssen et al. 2005). In the southwestern USA, an error of ±10% is usually achieved (Hendrickx and Hong 2005; Hong et al. 2009; Morse et al. 2000). Besides ET, SEBAL has been used to map biomass growth, water productivity and soil moisture (e.g. Alexandridis et al. 2009; Zwart and Bastiaanssen 2007).

2.2 Scale Dependency

Scale must be a fundamental consideration when geographers describe and explain spatial patterns and processes (Gibson et al. 2000), and is an especially important component of GIS analysis (Miller et al. 2007). As an important concept dealing with heterogeneity, scale dependency has been recognized in geography for decades (e.g. Bian and Walsh 1993; Meentemeyer and Box 1987; O'Neill et al. 1996; Turner et al. 2001; Wu 2004). These studies have improved our understanding on the scale effects in pattern analysis (Wu 2004). However, most of them merely report that scale effects exist, without studying their general patterns as landscapes change. In fact, Wu (2004) states that a general theory of scaling relations is yet to be developed.

It has been found that the effects of heterogeneity in vegetation on ET are significant when the resolution is high (Kustas et al. 2003). As spatial resolution decreases, the ability to determine flux variation decreases. More studies are needed on the spatial effects of ET modeling over heterogeneous landscapes (McCabe and Wood 2006).

It is necessary to understand the interaction between surface spatial variability in vegetation, the composite surface radiometric temperature and the resultant fluxes (Brunsell and Gillies 2003) when computing large-scale estimations of the surface energy balance. The processes governing the mass, energy, and momentum exchange across the land-atmosphere interface are nonlinear, because of the interdependence of the dominant variables and parameters (Brunsell and Gillies 2003). For example, the average value of a flux is not necessarily a function of the average value of the controlling variables and parameters (Brunsell et al. 2003). Moreover, the variability between fields is nonlinear, which results in poor aggregation values for mixed pixels unless sub-pixel information about cropping fraction is available (Kustas et al. 2004). Therefore, knowledge of the spatial distribution of the controlling variables is not adequate; rather it is more important to monitor how these distributions are altered when scale changes (Brunsell et al. 2003). When the spatial resolution of remote sensing data encompasses several land cover classes, the flux estimation can produce significant errors (Kustas and Norman 2000; Moran et al. 1997).

Upscaling (aggregation) of remotely sensed data is used in this dissertation to investigate scale dependencies (Hong et al. 2009). Hay et al. (1997) described upscaling as “resampling techniques designed to transform an image collected at a high spatial

resolution to a lower spatial resolution representation of the same image." During this process, the original raster data are downsized to fewer pixels with the same spatial extent (Hong et al. 2009). The statistical and spatial characteristics are modified in the aggregation process (Bian 1997). The spatial autocorrelation at coarser resolutions may be reduced since the total number of pixels is smaller (Bian 1997). Some studies show that when the spatial resolution is coarser, the data accuracy is higher (Carmel 2004; Van Rompaey et al. 1999). This higher accuracy occurs when the coarser resolution more closely matches the scale at which the pattern or process of interest occurs. Nevertheless, some information is lost in the spatial resolution downgrading process (Carmel et al. 2001).

Average-based methods have been used widely in the aggregation of input parameters in hydrologic models at the regional scale (Maayar and Chen 2006). Hong et al. (2009) find that simple averaging produces the most consistent and reasonable results. They also found that the standard deviation decreased when the aggregation level increased, which leads to the need to check the sensitivity of the results to input parameters before the aggregation method is applied (Hong et al. 2009).

2.3 Research Questions

Given the importance of energy flux in the hydrological cycle, there is a need to understand the interaction between surface spatial variability and the resultant fluxes, and how they vary with scale (Brunsell and Gillies 2003). There is, however, little understanding about the scale effect of ET. This paper addresses this research gap by studying the scaling relationships of land surface-atmosphere interaction and the

influence of landscape heterogeneity on ET. The primary purpose of this research is to explore how spatial heterogeneities in landscape influence surface flux exchanges with the atmosphere and to account for the scale dependency of ET estimation. Specifically, the study will seek answers to the following questions:

1. What effects do different aggregation techniques have on ET estimation as resolution decreases? How does landscape heterogeneity impact the aggregation process?
2. As major inputs to ET models, do the Normalized Difference Vegetation Index (NDVI) and surface temperature have consistent impacts on ET estimation across scales? Which input has a stronger correlation with ET estimation and does that correlation remain across scales of analysis?
3. How does the spatial autocorrelation of ET vary with scale? Does a relationship exist between the variance of spatial autocorrelation and spatial resolution?

The remainder of this thesis is organized as follows: Chapter Three introduces the study area, data and model used to estimate ET, and explains the methodology used to analyze the spatial pattern of ET. In the first part of Chapter Four, ET estimated from remotely sensed data are compared with measurements from eddy covariance towers. In the remainder of Chapter four, ET results from two aggregation techniques are compared, the correlations of NDVI and surface temperature with ET across scales, as well as the variogram analysis results are also presented. The last chapter summarizes and concludes the findings.

CHAPTER III

DATA AND METHODOLOGY

3.1 Site Description

The study site is at Freeman Ranch area. Freeman Ranch is used for ecological and agricultural research by Texas State University-San Marcos. It lies in Hays County, central Texas (Figure 3.1), with an area of 1,700 ha (29°56'N, 98°W). The climate is humid sub-tropical with mean annual temperature of 19°C (Dixon 2000). The summer highs are normally above 32°C and winter lows are near 4°C. An annual average precipitation of 86 cm is relatively evenly distributed over all months of the year (Dixon 2000). Elevation ranges from 204 to 287 meters above sea level, increasing from southeast to northwest (Carson 2000).

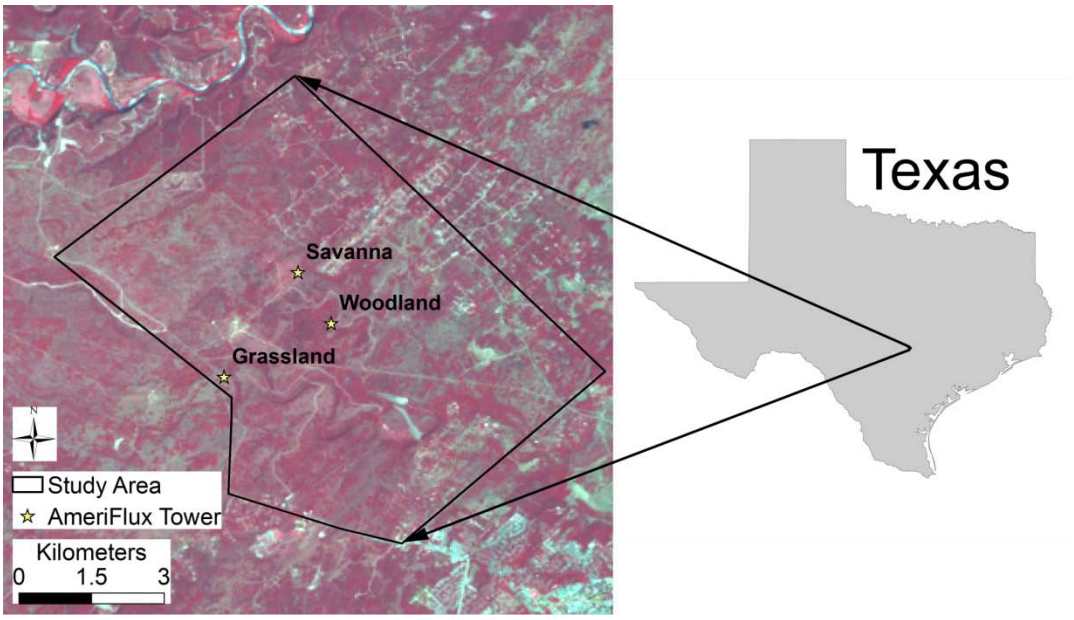

Figure 3.1 Location of the study area.

Major soil types identified are the Rumple-Comfort association and Comfort-Rock outcrop complex, which are both shallow soils developed over erosion-resistant limestone, covering more than 90% of the study area (Barnes et al. 2000). A detailed description of soil in this area is published by Carson (2000). Freeman Ranch has a great diversity of flora, encompassing more than 200 plant species. Plateau Live Oak (*Quercus virginiana var. fusiformis*) and Ashe juniper (*Juniperus ashei*) savannas are found in the uplands while closed-canopy woodlands grow in lowlands and intermittent drainages (Barnes et al. 2000). Woody plants (tree or shrub) cover approximately 48% of the landscape (Barnes et al. 2000), the most common of which is Ashe juniper. Herbaceous (usually grass-dominated) plants cover approximately 48% of the landscape, with the remaining 2% being non-vegetated surfaces such as roads, exposed rock, caliche outcrops, or buildings (Barnes et al. 2000). Two native perennial grass species are most common in these savannas: Texas wintergrass *(Nassella leucotricha)* and Texas grama (*Bouteloua rigidiseta*) (Barnes et al. 2000). Herbaceous

and woody cover types are found on all soils and terrains across the Freeman Ranch. However, woody plants are dominant on the shallow, rocky Comfort-Rock soils, whereas grasslands dominate the deeper Rumple-Comfort soils (Barnes et al. 2000).

3.2 Data Description

The purpose of this study is to identify a scaling relationship of ET derived from mainly remotely sensed data and ancillary data (Table 3.1). ET will be first calculated in the SEBAL model using remotely sensed data, elevation data, and ancillary meteorological data from a weather station. Then, ET estimations from the first step will be validated by eddy covariance measurements from AmeriFlux towers. Additionally, land cover information will be used in the spatial distribution analysis of ET.

Table 3.1 Data and their roles in this study

Data	Role	Source
LANDSAT 7	ET estimation	LANDSAT Program by USGS
DEM	ET estimation (elevation corrected temperature)	National Elevation Dataset by USGS
Meteorology	ET estimation	Weather station
Eddy covariance ET measurements	ET Validation	Ameriflux towers

Remote sensing data used in this study are from LANDSAT 7 satellite imagery. LANDSAT 7 was launched in 1999 and has eight bands with spectral range from 0.45 to 12.5 μm and a temporal resolution of 16 days. Its bands include a thermal infrared with 60 meter spatial resolution, six visible bands with 30 meter spatial resolution and a

panchromatic band with 15 meter spatial resolution. The thermal band is re-sampled to 30 meter by USGS after February 25, 2010 (Roy et al. 2010). The image scene size is 183 kilometers by 170 kilometers. The local equatorial time of satellite overpass is 10:55 am. A thorough introduction of this satellite can be found in the LANDSAT 7 Science Data Users Handbook (Irish 2000).

DEM data are from the National Elevation Dataset by USGS, and used to calculate elevation corrected temperature for ET estimation. Meteorological data needed in the model such as wind speed, relative humidity, daily minimum temperature and maximum air temperature, are collected by a weather station approximately eight kilometers to the southwest and obtained from the National Climatic Data Center website.

Validation data are from AmeriFlux eddy covariance sites located at Freeman Ranch. The AmeriFlux network was established in 1996 and provides regional and global micrometeorological observations used to study the impacts of climate and land-use change. Measurements at these sites are made using a three-dimensional sonic anemometer-thermometer and a fast response infrared gas analyzer, and include CO_2, water and energy fluxes. Eddy covariance methods are applied to calculate latent heat flux or ET. Goulden et al. (1996) did a rigorous evaluation of the precision and accuracy of eddy covariance technique, stating that this technique is effective for hourly, daily, monthly, and annual measurement with a precision of ±5%. Goulden et al. (1996) suggested that the eddy covariance technique is particularly well suited for testing remote sensing algorithms.

Three micro-meteorological towers at Freeman Ranch are located at grassland, savanna and juniper-oak woodland sites (as shown in Figure 3.1). Data are collected at half hour intervals and provide valuable measurements to verify SEBAL estimations for three land cover classes.

3.3 Methodology

This dissertation aims to study the scaling relationship of land surface-atmosphere interactions and the influence of landscape heterogeneity on ET across scales. The methodology consists of three parts, each corresponding to the research questions posed in previous chapters. First, I calculate ET at multiple spatial resolutions by (1) aggregating fine resolution ET estimates to coarser resolutions, and (2) aggregating raw LANDSAT images from a fine resolution to coarse resolutions and estimating ET with the aggregated raw data. Second, I analyze the correlation of ET with NDVI and surface temperature at each unique resolution. Third, I perform a semivariogram analysis to quantify the spatial autocorrelation of ET at various spatial resolutions and across multiple resolutions simultaneously.

3.3.1 Evapotranspiration Calculation from Remotely Sensed Data

3.3.1.1 Data Preprocessing

In this study, nine cloud free image scenes are used to estimate ET and validate SEBAL model performance. These images are calibrated and converted into surface reflectance and temperature in order to derive parameters for ET estimation in the

SEBAL model (i.e. surface albedo, NDVI, emissivity, surface temperature, net radiation, soil heat flux and sensible heat flux).

Image digital numbers (DN) are converted to radiance values, and then to top-of-atmosphere reflectance using the following two formulas.

$$L_\lambda = \text{gain} \times \text{DN} + \text{bias} \quad (1)$$

where L_λ is radiance and the gain and bias values are band specific rescaling factors (Table 3.3, from Chander et al. 2009). The images are acquired in low or high gain state. This state of high or low depends on the brightness of the surface. Low-gain is used for brighter surface, while high-gain for darker surface (Chander et al. 2009).

Table 3.2 LANDSAT 7 parameters

Band	Gain : (Wm^{-2} sr^{-1} m^{-1})/DN		Bias (Low) : (Wm^{-2} sr^{-1} μm^{-1})		$ESUN_\lambda$:(W m^{-2} μm^{-1})
	Low	High	Low	High	
1	1.180709	0.778740	-7.38	-6.98	1997
2	1.209843	0.798819	-7.61	-7.20	1812
3	0.942520	0.621654	-5.94	-5.62	1533
4	0.969691	0.639764	-6.07	-5.74	1039
5	0.191220	0.126220	-1.19	-1.13	230.8
6	0.067087	0.037205	-0.07	3.16	n/a
7	0.066496	0.043898	-0.42	-0.39	84.90

Radiance is then converted to top of atmosphere reflectance (ρ_λ), which removes variations due to differences in the solar zenith angle and Earth-Sun distance at different dates (Chander et al. 2009).

$$\rho_\lambda = \frac{\pi L_\lambda d_s^{\,2}}{ESUN_\lambda \cos\theta_s} \quad (2)$$

where ρ_λ is the planetary top-of-atmosphere (TOA) reflectance, d_s is the Earth-Sun distance, $ESUN_\lambda$ is mean solar exoatmospheric spectral irradiance (Wm^{-2} μm^{-1}) unique to each band, and θ_s is the solar zenith angle. A detailed description of the equations and explanations from DN to reflectance is available at Chander et al. (2009).

3.3.1.2 Evapotranspiration Calculation

SEBAL calculates ET as the residual of the surface energy balance equation (Bastiaanssen 1998)

$$\lambda ET = R_n - G - H \quad (3)$$

where λET is the latent heat flux, R_n is the net incoming radiant energy, G is the soil heat flux transferred into the ground, and H is the sensible heat flux induced by the temperature difference between surface and the overlying air. Each of these parameters is expressed in Wm^{-2}. The latent heat of vaporization of water (λ) is expressed in Jkg^{-1}.

R_n is computed from the TOA reflectance from band 1-5 and 7, as well as surface temperature from thermal band. G is estimated from R_n, surface temperature, and vegetation indices. H is estimated from surface temperature, surface roughness, relative humidity and wind speed (Allen et al. 2005). Parameters are calculated for each pixel using remotely sensed data at the instant corresponding to satellite overpass (Allen et al. 2005). A general schematic of the ET estimation process is illustrated in Figure 3.2. Equations for each parameter are listed and explained in the following paragraphs.

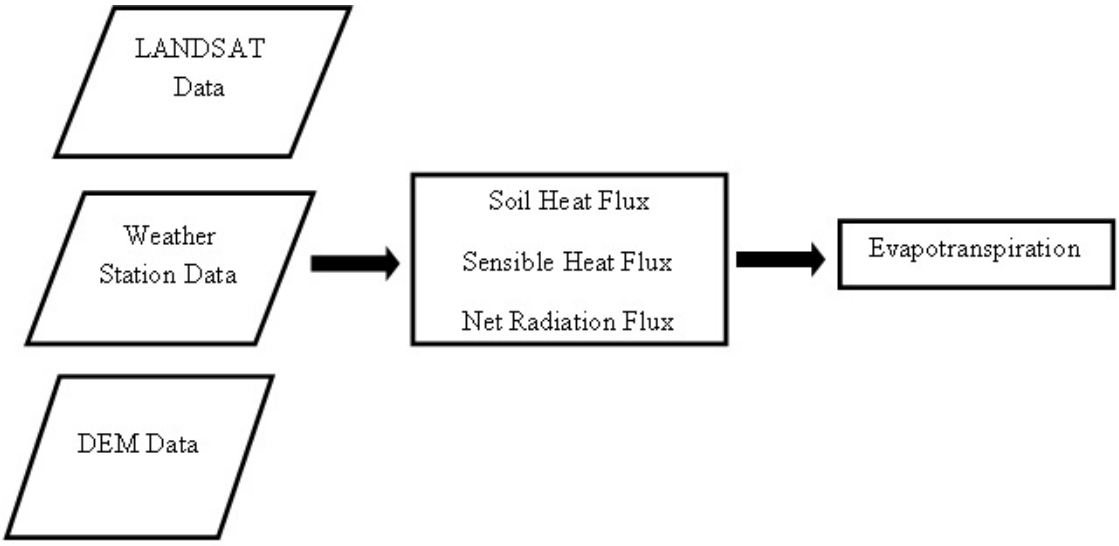

Figure 3.2 Schematic of the ET estimation process

Parameters (i.e., R_n, G, H) in the energy balance equation are calculated as indicated in the following formulas.

$$R_n = (1 - \alpha)R_s + \varepsilon_a \sigma T_a^4 - \varepsilon_s \sigma T_s^4 \quad (4)$$

$$\alpha = 0.356\rho_1 + 0.130\rho_3 + 0.373\rho_4 + 0.085\rho_5 + 0.072\rho_7 - 0.0018 \quad (5)$$

$$R_s = G_{sc} \cos\theta_s \, dsrt_{sw} \quad (6)$$

$$d_{sr} = 1 - 0.033 \cos\{[2\pi(DOY)/365]\} \quad (7)$$

$$\varepsilon_a = 1.08(-ln\tau_{sw})^{0.265} \quad (8)$$

$$\tau_{sw} = 0.75 + 2 \times 10^{-5} z \quad (9)$$

$$T_s = \frac{T_b}{\varepsilon_s^{0.25}} \quad (10)$$

$$T_b = \frac{K_2}{ln\left(\frac{K_1}{L_\lambda}+1\right)} \quad (11)$$

$$\varepsilon_s = 1.0094 + 0.047 \times \ln(NDVI) \quad (12)$$

$$NDVI = (\rho_4 - \rho_3)/(\rho_4 + \rho_3) \quad (13)$$

$$G = \left[\frac{T_s - 273.16}{\alpha}\left(0.0038\alpha + 0.0074\alpha^2\right)(1 - 0.98NDVI^4)\right] \times R_n \quad (14)$$

$$\mathrm{H} = \rho_{air} C_p \frac{dT}{r_{ah}} \quad (15)$$

$$\mathrm{dT} = \left(\frac{dT_{dry} - dT_{wet}}{Ts_{dry} - Ts_{wet}}\right) \times T_s - \left(\frac{dT_{dry} - dTwet}{T_{sdry} - T_{swet}}\right) \times T_{swet} \quad (16)$$

$$r_{ah} = \frac{ln(\frac{Z_2}{Z_1})}{u^* k} \quad (17)$$

$$u^* = \frac{u(z)k}{\ln\left(\frac{z - d_0}{z_m}\right)} \quad (18)$$

$$d_0 = 0.65\mathrm{h} \quad (19)$$

$$Z_m = 0.1\mathrm{h} \quad (20)$$

where R_s is the incoming short-wave solar radiation, α is surface albedo, τ_{sw}(-) is one way atmospheric transmissivity, ρ_i (i=1,3,4,5,7) is the reflectance of each band from LANDSAT 7, T_b is the brightness temperature (K), NDVI is the normalized difference vegetation index. r_{ah} is the aerodynamic resistances between two surface heights of surface and air temperature, Z_m is the roughness length, $u(z)$ is the wind speed (m/s)

at the height of z, h is the height for plant, d_0 is the zero displacement height, k is the von Karman constant (typically the value 0.41 is used), Z_1 is a height above the zero displacement distance height of plant canopy (set to 0.001), Z_2 is the reference height above the plant canopy, which is set to 2m, u* is the friction velocity, ρ_{air} is air density as a function of atmospheric pressure (mol m^{-3}), C_p is the heat of air at constant pressure with the value of 29.3 J mol^{-1} c^{-1}, dT is the near surface temperature difference (K), G_{sc} is the solar constant (1367 Wm^{-2}), and d_{sr} is inverse squared relative distance between the Earth and the Sun, DOY is day of the year, ε_a is the air emissivity, σ is the Stefan-Boltzmanh constant with the value of 5.67×10^8 Wm^{-2} K^{-4}, T_a is air temperature, T_s is the remotely sensed radiometric surface temperature, K_1 and K_2 are calibration coefficients with value of 666.09 and 1282.71 ($Wm^{-2}sr^{-1}\mu m^{-1}$) respectively, ε_s is surface emissivity.

H is estimated as a function of the wind speed, estimated surface roughness for momentum transport, and the near surface temperature difference between two heights (0.1 m and 2 m) (Hong et al. 2009; Tasumi et al. 2005). One wet pixel and one dry pixel are chosen in order to calculate H. The wet pixel is usually picked from a well irrigated area where the surface temperature is approximately to the air temperature. The dry pixel is picked from a dry area where λET is assumed to be zero. The selection of wet and dry pixel is aided with the spatial distribution of surface temperature measured by the thermal band of LANDSAT 7 (Bastiaanssen 1998). H is considered zero at the wet pixel and the difference between net radiation and soil heat flux at the dry pixel. At the dry pixel, dT is a function of the sensible heat flux. At the wet pixel, dT is assumed to be zero. dT is computed with assumption of a linear relationship for the rest pixels of the image (Kite

and Droogers 2000). Values at these two pixels are used for an internal calibration to reduce biases of other parameters used in SEBAL (e.g. albedo, net radiation, surface temperature) (Hong et al. 2009). Since there is no irrigated area in the study area, the wet pixel is instead selected in forested areas that have the lowest temperatures. Specifically, pixels with lower surface temperatures are identified. Then, many wet pixel candidates are selected from among the filtered pixels that occur in forests. These pixels were iteratively tested as the wet pixel to examine the impact of different wet pixels on ET estimation. Negligible differences in ET resulted from these tests and it was determined that any of the lowest temperature pixels occurring in forests were adequate representations of the wet pixel required by SEBAL.

Instantaneous ET at the time of satellite overpass will be calculated from the equations above. Longer temporal aggregations of ET (e.g., daily, monthly or annual ET) are more meaningful for metrological and hydrological studies. In this study, daily ET is used for the identification of scaling relationships. Daily ET is computed by the daily-averaged net radiation flux, the soil heat flux and the instantaneous evaporative fraction (EF), with the assumption that EF is equal to the daily mean value when the satellite is passing over (Bastiaanssen 1998; Farah et al. 2004; Gentine et al. 2007). The soil heat flux is assumed to be zero at the daily scale (Kustas et al. 1993). Daily ET (ET_{24}) can be calculated as (Bastiaanssen et al. 2005):

$$ET_{24} = \frac{86{,}400 10^3 EF R_{n24}}{\lambda \rho_w} \quad (21)$$

$$EF = \lambda ET / (R_n - G) \quad (22)$$

$$R_{n24} = (1 - \alpha)R_{s24} + L_{24} \quad (23)$$

R_{n24} is the daily-averaged net radiation (Wm^{-2}), which is obtained from a meteorological station and then interpolated using the distributed albedo values. ρ_w is the density of water (kgm^{-3}). EF is instantaneous evaporative fraction. Rs_{24} is the daily average incoming solar radiation. L_{24} is the daily average net long-wave radiation.

3.3.2 Aggregation Process

ET will be first calculated at the 30m resolution of original data. Then all input data for ET calculation and output ET calculated at 30m will be (re)scaled to the following resolutions: 60m, 120m, 240m, 480m and 960m. The finest resolution is equivalent to the resolution of the LANDSAT 7 spectral bands (~ 30m) and the coarsest one is similar to the MODIS thermal band (~ 1000m). The scaled values will be the mean value of all pixels falling within an *n* by *n* window of the finer resolution data (Hong et al. 2009). Resolutions between these two endpoints will be used to evaluate the aggregation effects at different scales.

In the aggregation process, two methods can be followed: run the model first and then aggregate the output or aggregate the input data first and then run the model (Addiscott 1993; Heuvelink and Pebesma 1999). These two methods are shown in Figure 3.3. These two methods would yield same results if the model is linear (Addiscott 1993).

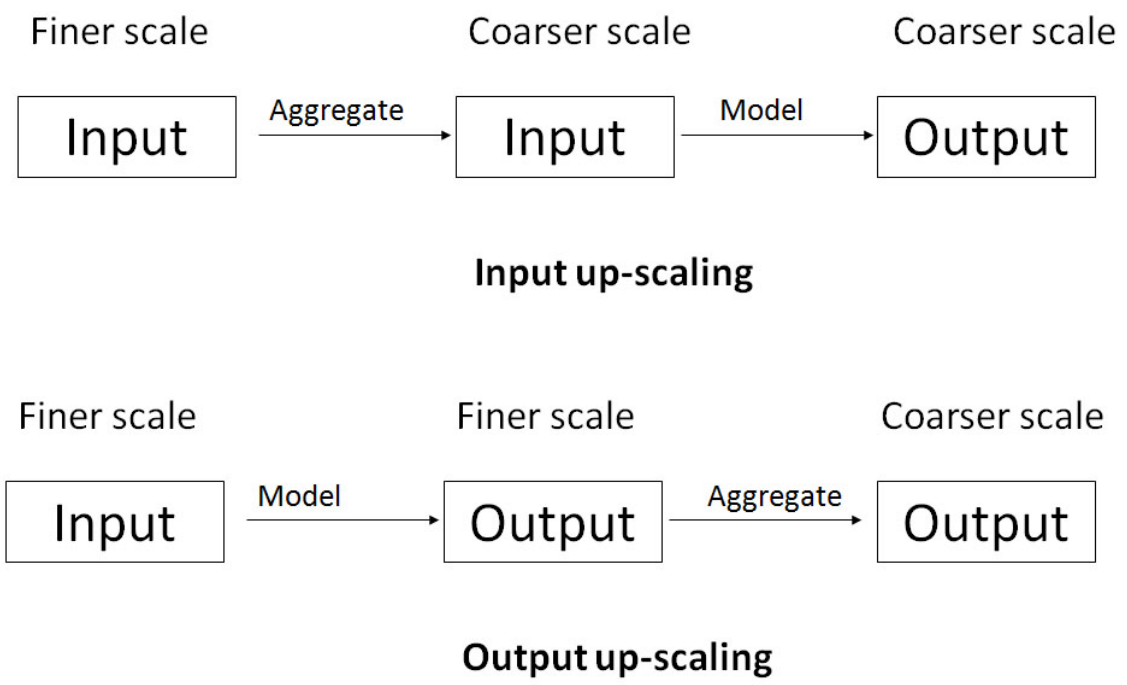

Figure 3.3 Two methods of aggregation: input up-scaling and output up-scaling.

ET will be estimated at resolutions of interest using the two methods mentioned above. In the first method, all parameters (e.g. vegetation indices, surface temperature, and albedo) will be aggregated from 30m to coarser resolutions before SEBAL is applied. Then ET will be calculated from the aggregated data at various resolutions. In the second method, ET will be calculated first at 30m resolution using SEBAL and then aggregated to coarser resolutions. It would make no difference if the combined impact of all factors on ET is linear. However, current literature finds that ET does not scale linearly due to all the factors impacting it, leading to uncertainties associated with its calculation. Ferguson et al. (2010) identified three important sources of uncertainty in ET estimation, which are vegetation parameterization, surface temperature and the source of net radiation data. To analyze this uncertainty caused by ET driving forces, ET derived from the first method will be compared with ET derived from the second method. It is expected that results

from this comparison will highlight the impact of these factors on ET estimation at multiple scales.

ET results from two methods will be compared in the following aspects: basic descriptive statistics, histograms, pixel by pixel differences and spatial pattern. Basic statistics and histograms will be used to compare ET distributions derived from the two methods, and pixel by pixel difference will reveal the spatial locations of differences. Two landscape metrics will be calculated to compare spatial patterns that derive from the different methods of aggregation: Number of Patches (NP) and Patch Ratio (PR). NP calculates the number of patches in the landscape (McGarigal et al. 2012). PR the ratio of the number of patches (NP) divided by the total number of pixels. Since these metrics only work with categorized data, ET will be recoded into the following categories (Table 3.3).

Table 3.3 ET recoding rule

Original ET (mm/day)	Recoded ET (mm/day)
0-1	1
1-2	2
2-3	3
3-4	4
4-5	5
5-6	6

3.3.3 Correlation Analysis across Scales

To determine if NDVI and surface temperature have consistent correlations with ET estimations across scales, ET will be separately regressed on NDVI and surface temperature at each resolution (30m, 60m, 120m, 240m, 480m, and 960m) and the coefficients of determination will be compared.

3.3.4 Geostatistical Analysis

As mentioned earlier, some patterns exist or are visible only at certain scales, and spatial resolution plays an important role in the identified pattern. To study the impact of the spatial resolution of remotely sensed data on the spatial autocorrelation of ET, a geostatistical analysis will be performed. A semivariogram is a geostatistical function that describes the degree to which nearby locations have similar values, and is diagnostic of scene structure (Woodcock et al. 1988). It has been widely used in digital processing to study spatial structures (Atkinson and Lewis 2000; Curran 1988; Warren et al. 1990). The definition of an experimental semivariogram is "half of the average squared difference between values separated by a given lag, which is a vector in both distance and direction" (Atkinson and Lewis 2000). It is calculated as

$$2\gamma\,(d) = \frac{1}{n(d)} \sum_{d_{ij}=d} (Z_i - Z_j)^2 \qquad (20)$$

where γ is the conventional symbol for the semivariogram, *d* stands for distance, Z_i represents the value of the parameter at point i, and γ (*d*) is a function of distance *d,* determined by "the average sum of squared differences in attribute values for all pairs of control points that are a distance *d* apart" (Lightowlers et al. 2008). The number of pairs

of points at separation *d* is n(*d*) (O'Sullivan and Unwin 2002). When the distance *d* increases, semivariance is inclined to increase from zero to the value of the global variance for the image, and then remains constant afterward (O'Sullivan and Unwin 2002). Since semivariance is half of the variance, they are both interchangeable in this dissertation.

Models are created to fit the empirical semivariogram, common ones including periodic, linear, circular, spherical, Gaussian, exponential and so on (Cressie 1991). For example, the periodic shape of the semivariogram displays a repeating pattern where the semivariance of pixels from greater distances is smaller than the semivariance of pixels from near distances, an example of which is rows in crop lands. Another model is the linear model, which rises constantly and does not have a range (Levesque and King 1999).

The graph shown in Figure 3.4 is from a spherical model, which is typical of an image having pixels totally independent beyond the range (Levesque and King 1999). The nugget is the variance at the distance of zero. The range, also called lag, describes the distance at which the semivariogram becomes even and constant (Lenz and Baise 2007). This distance is impacted by the size of objects in the image. The sill is the constant semivariance value beyond the range (O'Sullivan and Unwin 2002). The difference between sill and nugget is called partial sill, which represents the variance of a spatially autocorrelated process without any nugget effect. Semivariogram analysis will be performed on ET at resolutions from 30m to 960m. By examining the nugget, range and partial sill values of each variogram across scales, the semivariance is expected to relate to the spatial resolution.

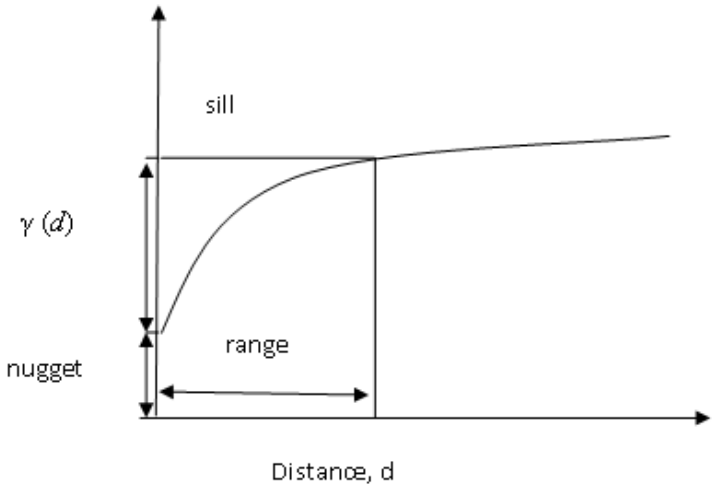

Figure 3.4 Typical fitted variogram, with key features-the sill, nugget and range.

The heterogeneity of landscape has an impact on the variance of a spatially autocorrelated process. A heterogeneous landscape has more than one land cover classes. Neighboring pixels that belong to the same land cover class form a patch. When the pixel size or spatial resolution is smaller than the patch size, many pixels are pure. According to the law of geography: “Everything is related to everything else, but near things are more related than distant things” (Tobler 1970), the variance is small. When the resolution becomes coarser, the number of pure pixels decreases while the number of mixed pixels increases. The variance value is bigger. When the resolution coarsens to a certain extent, there are many mixed pixels, or to an extreme, all pixels are mixed. The variance value becomes random, and hard to predict.

CHAPTER IV

RESULTS AND DISCUSSIONS

This dissertation addresses questions of scale by studying land surface-atmosphere interactions and the influence of landscape heterogeneity on ET across scales. When the spatial resolutions change from finer to coarser, what impact does landscape heterogeneity have on the pattern of ET? To answer this question, the research is conducted from three aspects: the effect of aggregation techniques, the correlation between ET and its indicators across scales, and the relationship between spatial autocorrelation and spatial resolution.

This chapter is organized as follows. Section 4.1 validates the ET estimations from remotely sensed data with the field measurements from eddy towers. Section 4.2 studies the temporal and spatial relationship of ET with several factors including length of day, land cover, surface temperature and vegetation indices at the finest scale-30m. Section 4.3 compares two ET aggregation techniques across scales. Section 4.4 studies the correlation between surface temperature, NDVI and ET across scales. Section 4.5 studies the spatial autocorrelation by conducting the semivariogram analysis at various resolutions.

4.1 Validation of Evapotranspiration calculated from Remotely Sensed Data

Remote sensing based ET estimates at 30 meter resolution were compared with eddy covariance ET measurements for 9 dates, ranging from March to December, to ensure the reliability of the remote sensing estimates (Table 4.1, Figure 4.1). The specific dates cover seven months in the year 2005 excluding January, February, May, July and August. All of these images were taken at 10:55 am local time. Images for the missing months all have more than 70% cloud cover making it impossible to get reliable ET estimates from those images. The absolute maximum ET estimate amongst all images occurred on June 14 and the absolute minimum ET estimate amongst all images occurred on September 18. The highest mean value was on June 14 and lowest mean value on December 23. Unit of ET estimations in this dissertation is mm/day.

Table 4.1 Statistics of ET on nine dates

Date	DOY	ET min	ET max	ET mean
03/10/05	69	0.10	5.21	2.80
04/11/05	101	0.04	6.77	4.16
04/27/05	117	0.81	7.69	5.07
06/14/05	165	1.65	8.88	5.67
09/18/05	261	0.01	5.98	3.87
10/20/05	293	0.23	3.96	2.59
11/05/05	309	0.02	3.39	1.92
11/21/05	325	0.20	2.94	1.89
12/23/05	357	0.13	3.08	1.70

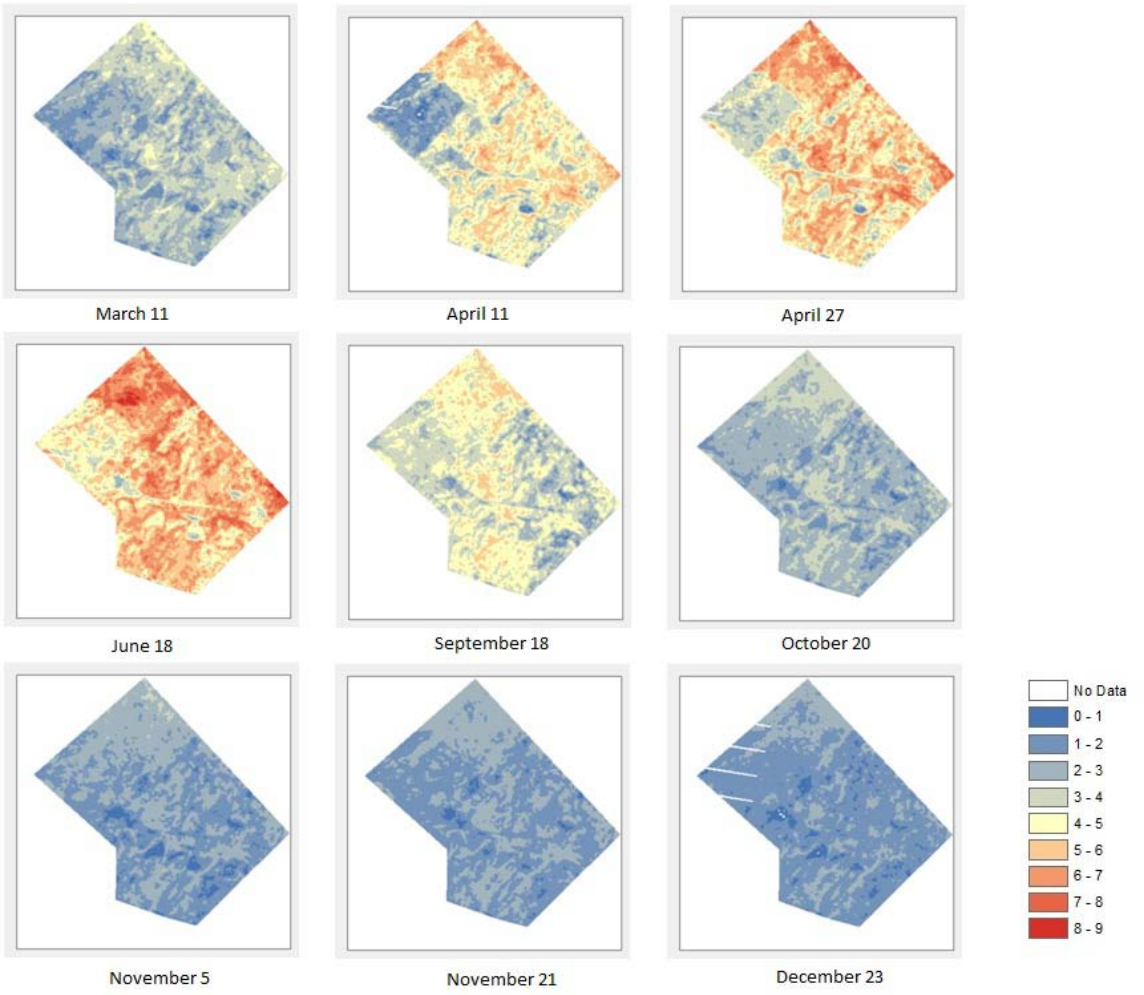

Figure 4.1 Daily ET maps from nine dates.

Validation data are from three eddy covariance towers located at Freeman Ranch, Texas. Before comparing ET from remotely sensed data and the eddy covariance measurement tower, the footprint of eddy tower measurements must be determined. The extent of the effective footprint of flux depends on wind direction, wind speed, surface roughness and atmospheric stability (Schmid 2002). Eddy covariance tower measures ET every half hour, and the footprint for that measurement can change during the day with variable winds and directions (Hong 2008). The range of flux can go from ten to a hundred meters (Sun et al. 2011). When used for the validation of ET from remote

sensing imagery, the commonly used footprint for daily measurements from eddy covariance measurement towers is usually set at one pixel size on the LANDSAT 7 imagery (30m×30m)(Li et al., 2008). Measurements are taken at half hour intervals at these sites. The measurements taken at closest to the LANDSAT overpass time were selected, which is at 11:00am. Table 4.2 shows daily ET estimates from LANDSAT 7 (as SEBAL) and eddy covariance measurements (as flux tower).

Table 4.2 Daily ET from LANDSAT 7 and eddy covariance towers

Date	DOY	Grassland		Woodland		Savanna	
		Flux tower	SEBAL	Flux tower	SEBAL	Flux tower	SEBAL
3/10	69	2.7	1.9	2.9	3.2	2.4	1.6
4/11	101	3.0	2.7	3.2	4.6	3.1	2.3
4/27	117	3.6	4.0	3.1	5.7	3.1	4.1
6/14	165	4.0	4.5	4.2	5.7	4.7	5.1
9/18	261	3.8	2.9	3.7	3.8	3.4	3.6
10/20	293	1.5	1.8	1.4	2.9	1.7	1.4
11/5	309	0.7	1.1	1.1	2.2	1.4	0.9
11/21	325	1.0	1.4	0.7	2.0	0.9	0.9
12/23	357	0.2	1.2	0.2	1.9	0.4	0.8

ET measured with the eddy covariance technique were regressed on satellite-based ET estimates. Regression results reveal that ET from remotely sensed data has a high R^2 at each of the three sites. The R^2 values for each site are 0.81(grassland), 0.76 (woodland) and 0.86 (savanna) (Figure 4.2).

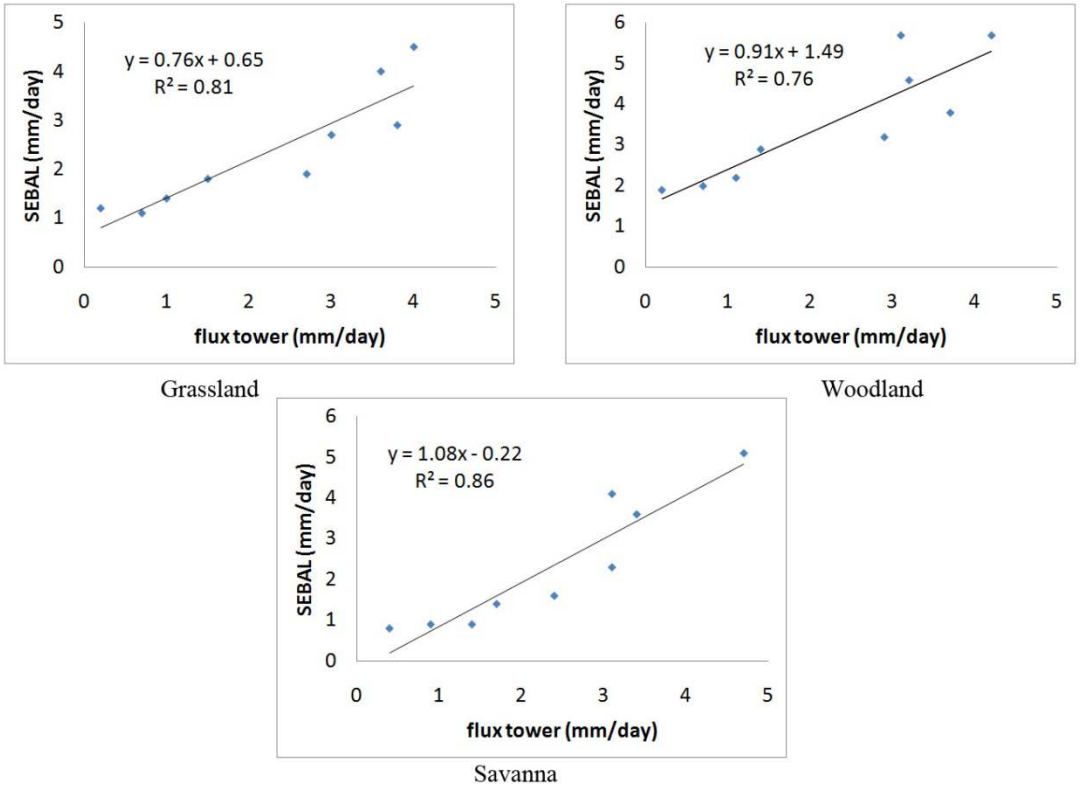

Figure 4.2 Regressions of ET at three sites.

The overall regression at three sites is shown in Figure 4.3 with an R^2 of 0.67. The overall R^2 is smaller than individual R^2 at three sites. This finding suggests that validation of ET calculated from SEBAL should be performed based on individual land cover class, instead of grouping all locations together.

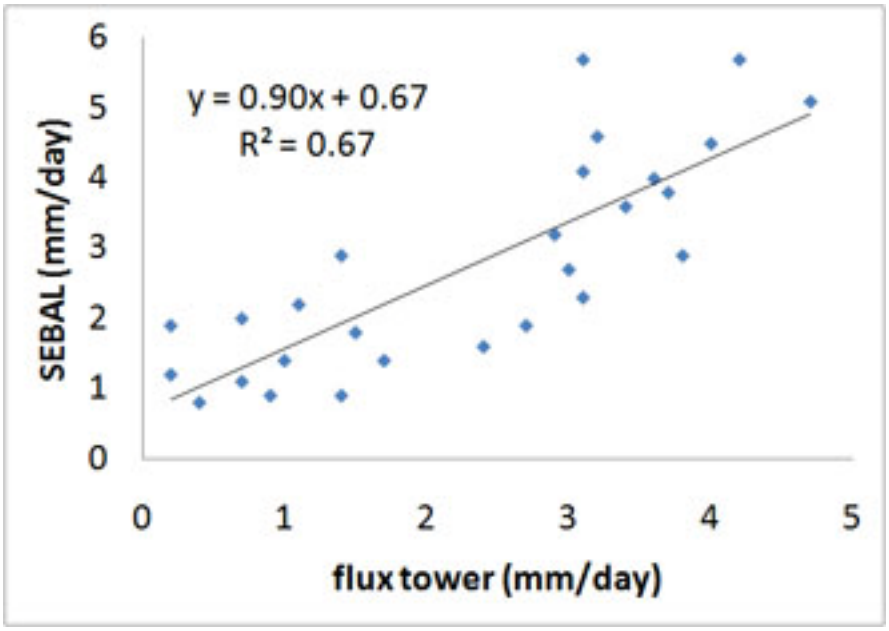

Figure 4.3 ET validations at three sites.

ET values from nine dates are plotted to evaluate the temporal performance of the SEBAL model (Figure 4.4). In general, flux tower measurements reflect the temporal trend of SEBAL estimates at all three sites.

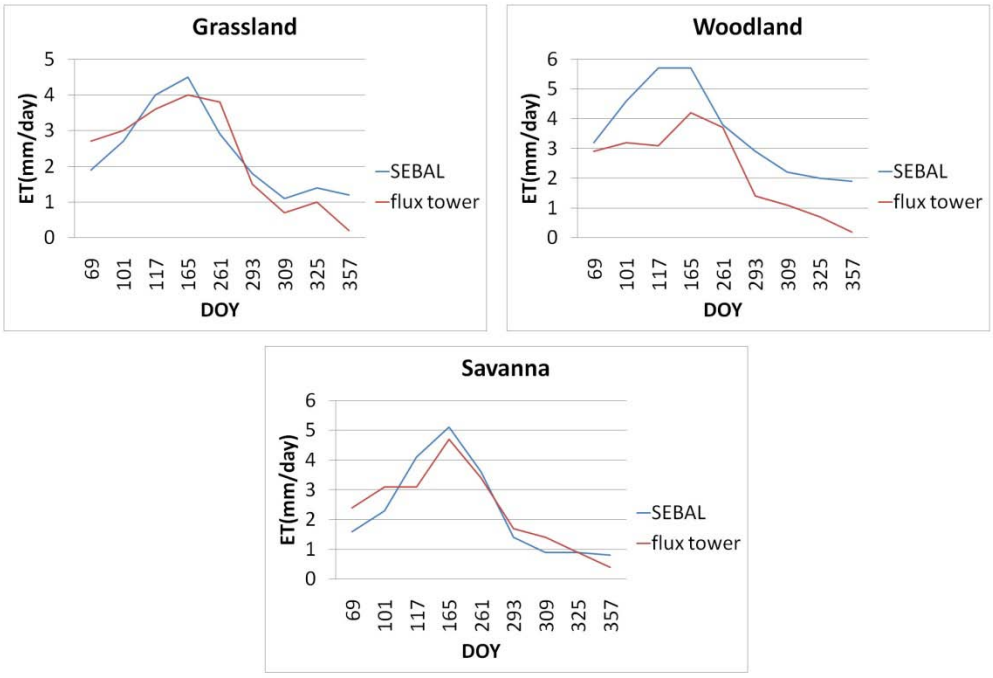

Figure 4.4 Validation of ET values for nine dates at three sites.

ET at the grassland site increased from Day 69, and peaked on Day165, dropped to the lowest value on Day 309, increased again on Day 325, and dropped to the lowest value on Day 357. At the grassland site, SEBAL underestimated ET on Day 69, 101 and 261. At the woodland site, ET estimated by SEBAL peaked on Day 117, and was almost the same value on day 165, when flux tower got to its peak. After Day 165, ET from both methods begins to drop and the lowest value was on Day 357. SEBAL overestimated ET for all the dates studied at this site. ET at the savanna site increased from Day 69, and peaked on Day165. The lowest value was on Day 357. SEBAL overestimated ET on Day 117, 165, 261, and 357.

Although ET estimates from remotely sensed data do not perfectly match eddy covariance measurements, the trends have a high degree of similarity. The high R^2 shows that ET estimates from remotely sensed data are sufficiently accurate to justify their use in this study, since 76%-87% of the variation in ET measurements from eddy covariance towers are reflected by ET estimates from remote sensed data.

4.2 Spatio-temporal Patterns of Evapotranspiration

ET varies spatially and temporally due to variations of external drivers (e.g. climate, soil moisture) and internal drivers (e.g. vegetation) heterogeneity (Foley et al. 2003; Verstraeten et al. 2008; Wear and Greis 2002). In this subsection, ET is compared with several factors including length of day, surface temperature, land cover, and NDVI for the purpose of exploring their temporal and spatial relationships with ET. Soil moisture is not included in this study because of its strong correlation with ground and

surface temperature, due to the energy exchange via latent heat and sensible heat (Goward et al. 1985).

4.2.1 Temporal Pattern of Evapotranspiration

No significant change of land cover classes occurred in 2005. Thus, land cover data are not used to study the temporal trend of ET. Instead, parameters including surface temperature (T), NDVI, and length of day vary daily and seasonally, and were calculated to study their temporal relationships with ET (Table 4.3).

Table 4.3 Statistics of ET, NDVI, surface temperature, and length of day

DOY	Mean ET (mm/day)	Mean NDVI	Mean T (°C)	Length of day (hrs)
69	2.79	0.41	22.39	11.83
101	4.16	0.47	26.52	12.80
117	5.07	0.46	29.02	13.23
165	5.67	0.49	28.14	14.07
261	3.87	0.49	30.02	12.25
293	2.59	0.46	26.8	11.32
309	1.92	0.43	25.02	10.88
325	1.89	0.43	18.91	10.52
357	1.70	0.39	16.53	10.23

Figure 4.5 plots the length of day, mean surface temperature (T), and mean NDVI, with mean ET value on 9 dates in the year 2005. Comparing these three graphs, the temporal trend of ET corresponds best with length of day. They both increase from

day 69 to day 165 and then decrease all the way to day 357. Length of day is an indicator of the radiation from the Sun, which is the energy source for the ET process. Seasonally speaking, ET and length of day (solar radiation) increase from spring to summer, and drop from summer to fall and winter. This also corresponds with patterns of vegetation phenology, while part of ET is from leaf transpiration. When fall comes, leaves begin to senesce and most vegetation becomes dormant.

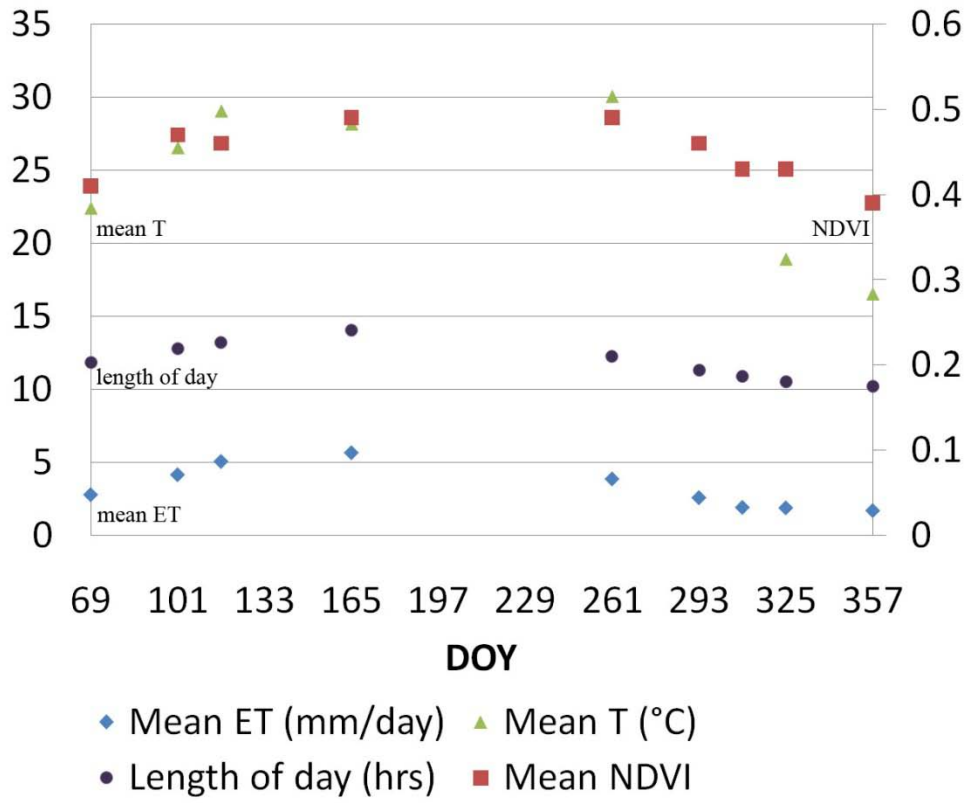

Figure 4.5 The length of day, mean surface temperature, mean NDVI and mean ET values on nine dates in the year 2005.

The general temporal trends of ET, mean surface temperature and NDVI are similar. They go up from the beginning of the year to the middle of the year and then drop to the end of the year. However, their peak dates are different. ET has the highest

value on day 165, while the highest mean surface temperature is on day 261, the highest mean NDVI on day 165 and 261.

The relationship between temporal trends identified visually is echoed in the coefficient of determination. R^2 between mean ET and the length of day, mean surface temperature, and mean NDVI were 0.97, 0.57, and 0.61 respectively. R^2 for length of day and ET was much more than R^2 for surface temperature and NDVI. This result reveals that the length of day has the strongest temporal relationship with ET, because the energy source of ET is solar radiation. There might be a several days lag between ET, NDVI, and temperature. However, the time range is at least 16 days in this study which is not sufficient to validate this assumption.

4.2.2 Spatial Pattern of Evapotranspiration

Remotely sensed data reflect the character of the type, amount and condition of vegetation (Jackson and Huete 1991). Vegetation index, derived from multiple bands by mathematical manipulations, measures biomass or vegetative vigor (Jackson and Huete 1991), including NDVI, EVI, NDWI and so on. NDVI is the most popular one used by scholars, as an indicator of photosynthetic activity of plants, vegetation cover, and biomass production (Gamon 1995; Karaburun 2010; Sellers 1985). The spatial distribution of surface temperature, vegetation indices, and land cover are analyzed to find their relationships with ET beginning at the finest resolution (30m) and other resolution aggregates. This analysis is done to answer the second research question: Do the ET-NDVI and ET-Temperature relationships vary with scale? ET from September 18, 2005 was selected to study the spatial scale effects. It was chosen because all pixels have positive values and the LANDSAT 7 dataset is complete. Daily ET at Freeman Ranch on

September 18, 2005 ranged from 0.01 to 5.98 mm/day (Figure 4.6). The mean, median, mode values are 3.87 mm/day, 3.92 mm/day, 4.23 mm/day with the standard deviation as 0.85.

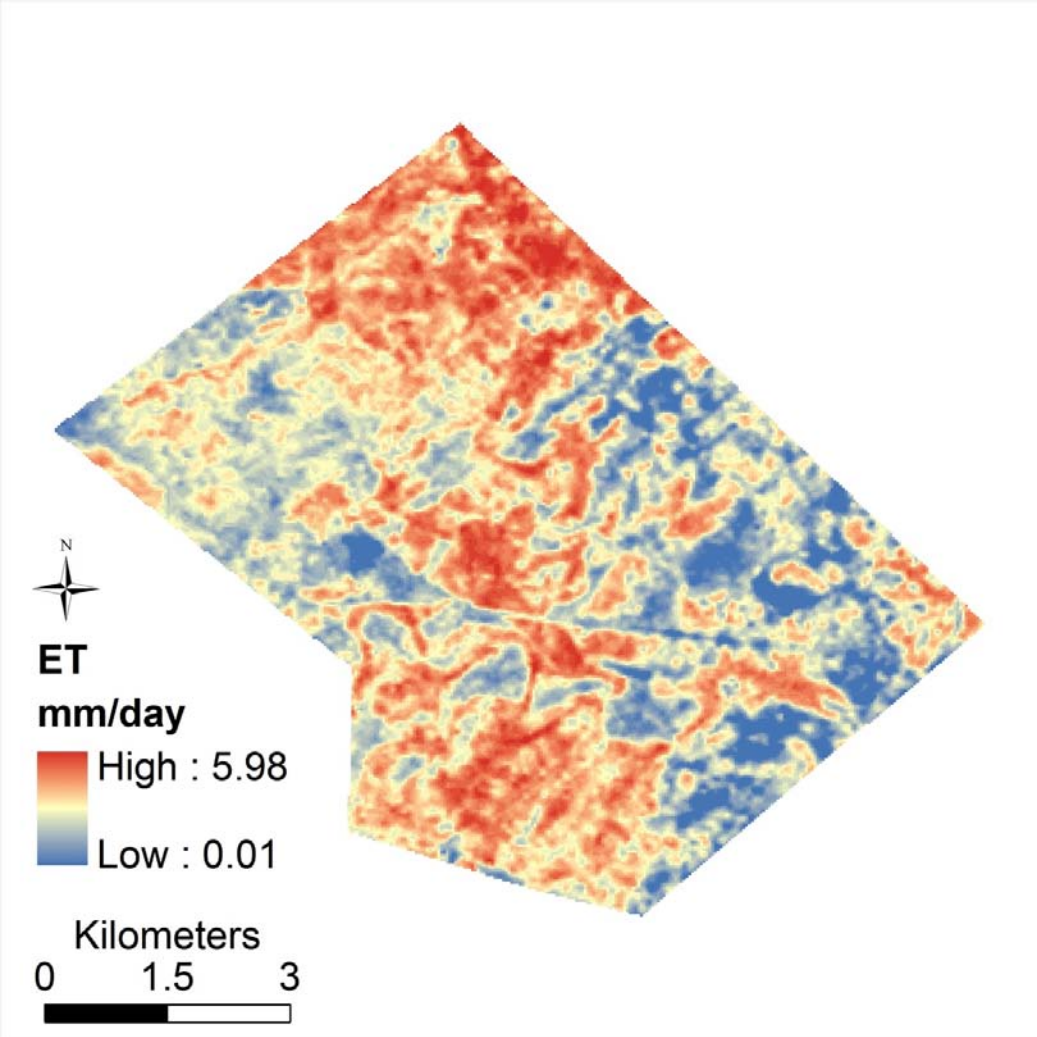

Figure 4.6 Spatial distribution of ET.

The spatial distribution of surface temperature for the study site is displayed in Figure 4.7. The highest and lowest surface temperatures were 36.3°C and 27.3°C respectively, with the mean and mode values both as 30.0°C, the median as 30.3°C. The standard deviation is 1.27. The west and east parts of the study site had higher

temperatures than the central part. The land cover map shows that west and east are mainly grassland and shrub, while the central part is mostly forest. In general, the distribution of surface temperature corresponds with that of ET, while the higher the surface temperature, the lower the ET and vice versa.

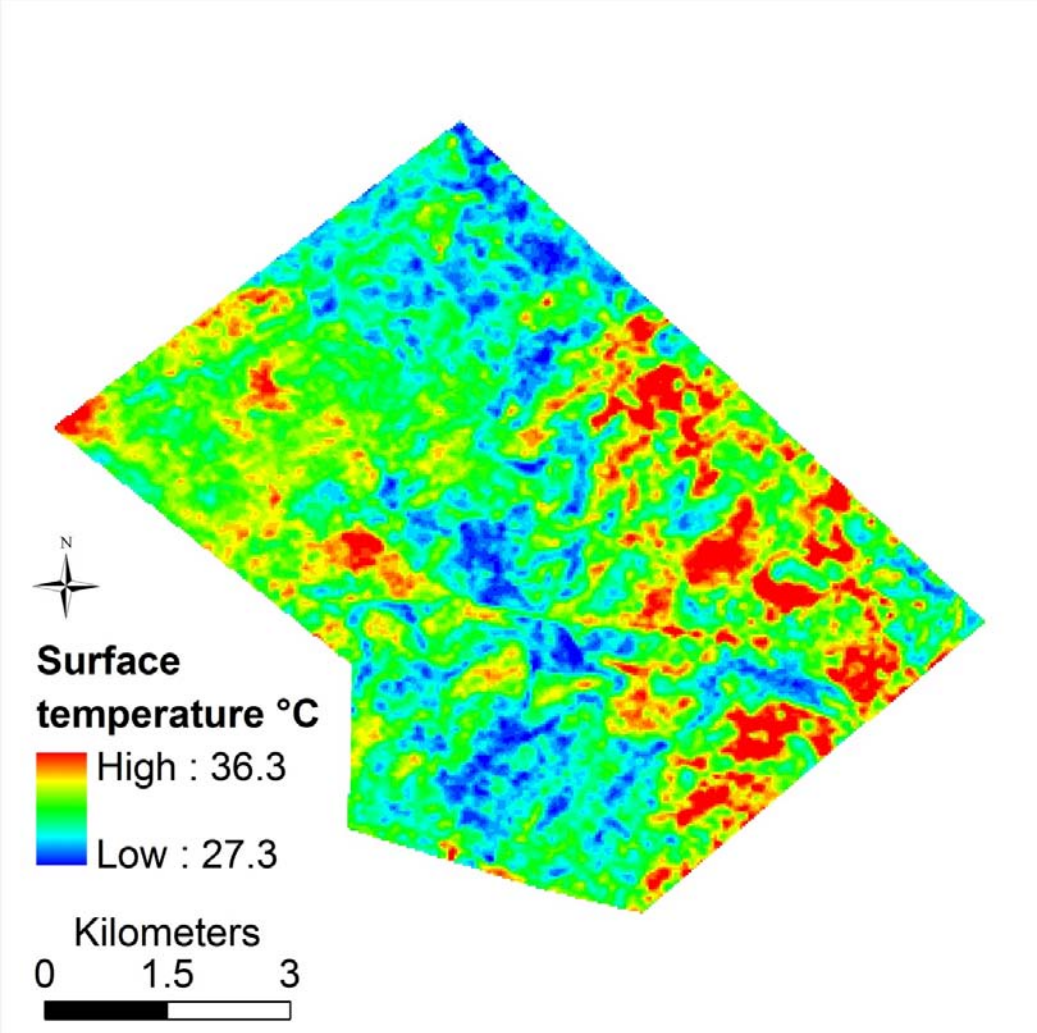

Figure 4.7 Spatial distribution of surface temperature.

The spatial distribution of NDVI is displayed in Figure 4.8. The Value of NDVI ranges from 0.14 to 0.69, with the mean, median, and mode values of 0.49, 0.50 and 0.55, respectively. The standard deviation was 0.07. In general, the distribution of NDVI

corresponds with that of ET, while the higher the NDVI value, the higher the ET and vice versa.

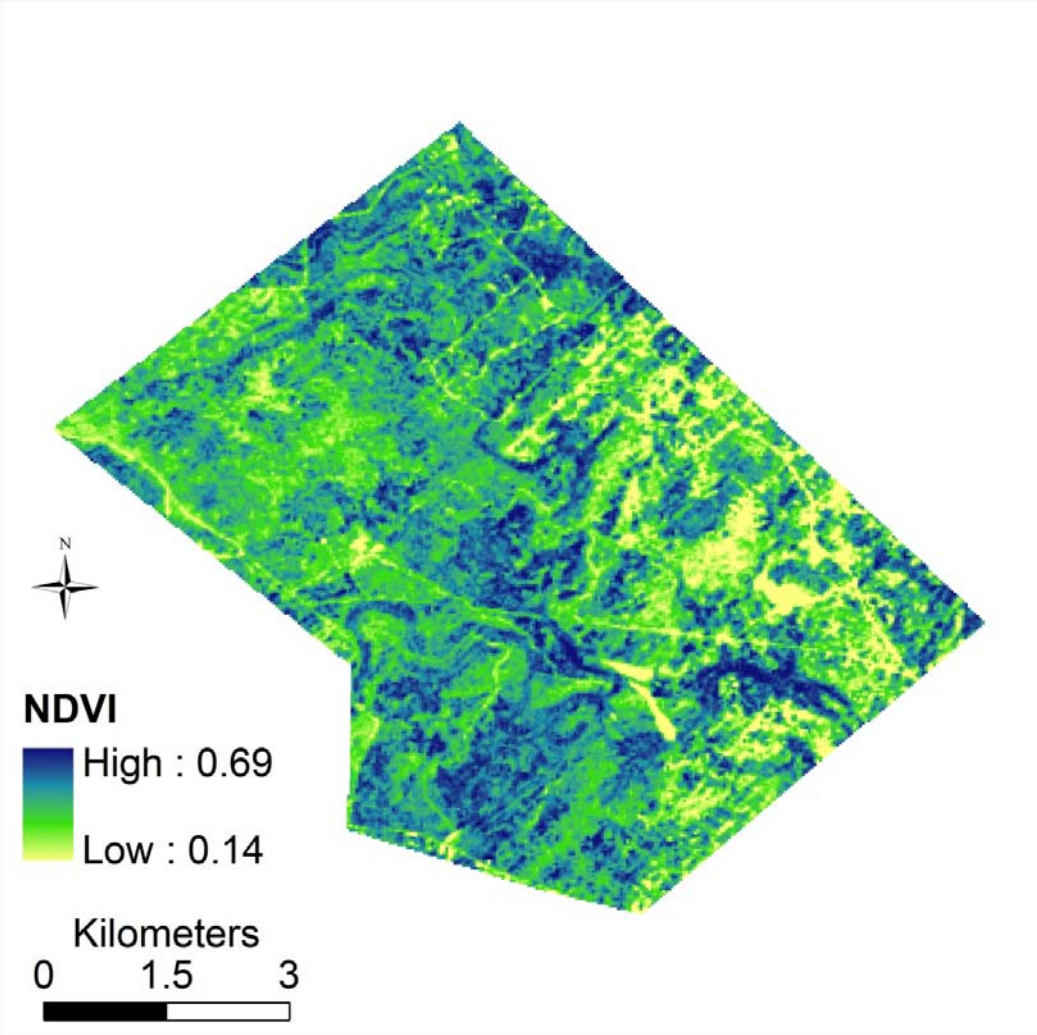

Figure 4.8 Spatial distribution of NDVI.

A supervised classification using the maximum likelihood method was performed to create the land cover map, with classes including: forest, shrub/scrub, grassland/herbaceous and non-vegetated surfaces. Non-vegetated surfaces include bare soil and built-up areas. Training samples for classification were derived using the 2006 NLCD (National Land Cover Database) product and 1 meter resolution NAIP (National Agriculture Imagery Program) imagery as reference map. A sample of sixty points were

randomly sampled to assess the classification accuracy (Table 4.4). The Overall Classification Accuracy is 80.00%. Land cover map of Freeman Ranch and map of ET are displayed in Figure 4.9. Forest, shrub, and grassland in total take up 94.45% of land at Freeman Ranch (Table 4.5).

Table 4.4 Accuracy of land cover classification results

Class name	Reference totals	Classified totals	Number correct	Producers accuracy	Users accuracy
Forest	21	24	20	95.24%	83.33%
Shrub/scrub	13	10	8	61.54%	80.00%
Grass/ herbaceous	17	16	13	76.47%	81.25%
Non-vegetated	9	10	7	77.78%	70.00%

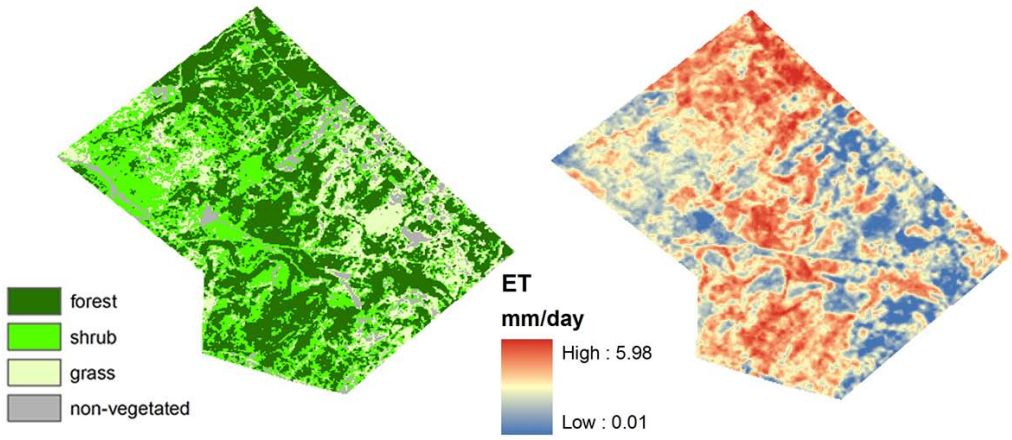

Figure 4.9 Land cover and ET.

Table 4.5 Percentage of each land cover

ID	Land cover	Count	Percentage
1	Forest	22728	42.19%
2	Shrub/scrub	18222	33.82%
3	Grassland/ herbaceous	9919	18.41%
4	Non-vegetated surfaces	3006	5.58%

Landscape metrics were computed for the entire land cover. There were 2513 patches in total, covering one to more than six thousand pixels. The mean patch sizes for forest, shrub, grass and non-vegetated surfaces were 51, 14, 19, and 8 pixels. The mean patch size for the entire area was about 22 pixels.

Comparing land cover and ET maps, the spatial pattern of ET matches that of the land cover. This matching pattern was most apparent at forest areas, where ET exhibited a pattern nearly identical to the shape of the forest. The spatial patterns of ET at the other three land cover classes do not display a strong coincidence with land cover classes. ET at each land cover class is summarized in Figure 4.10. ET from non-vegetated surfaces was lowest, 2.61 mm/day, followed by grassland/herbaceous, and the highest ET was from forest, 4.53mm/day. Forest has the lowest temperature and highest NDVI whereas non-vegetated surfaces have the highest temperature and lowest NDVI. For a particular land cover class, high ET would come with high NDVI and low surface temperature.

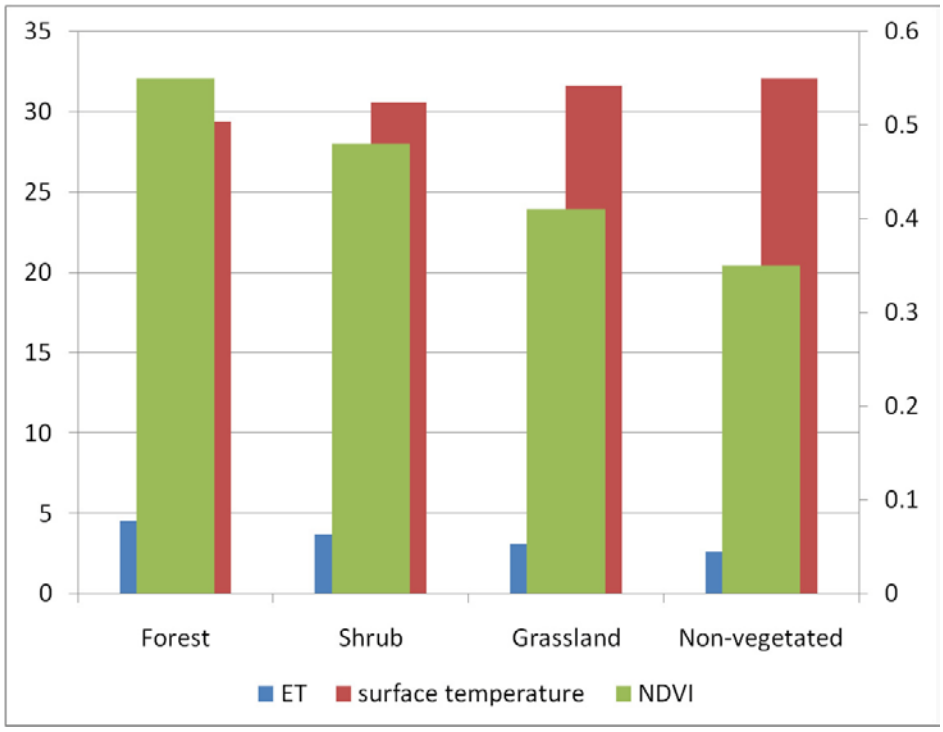

Figure 4.10 Mean daily ET, surface temperature and NDVI by land cover class.

4.3 Scaling Relationship of Evapotranspiration

This section explores the spatial scaling relationship of ET across scales including pixel resolutions at 60m, 120m, 240m, 480m and 960m. The purpose is to answer the questions stated in earlier: What effects do different aggregation techniques have in ET estimation as resolution is decreased? How does landscape heterogeneity impact the aggregation process? As major inputs to ET models, do the NDVI and surface temperature have consistent correlation with ET estimation across scales? Which input has a stronger correlation with ET estimation and does that correlation remain across scales of analysis? How does the spatial autocorrelation of ET vary with scale? Is there a relationship existing between the variance of spatial autocorrelation and the spatial resolution?

4.3.1 Evapotranspiration Calculated from Two Aggregation Techniques

Two types of ET maps are created using different aggregation techniques. The first technique is to average SEBAL-derived ET estimates from 30 meters to coarser resolutions. These results are called output up-scaling ET. The second technique is to average LANDSAT 7 reflectance bands from 30 meters to coarser resolutions and then calculate ET from the aggregated images using SEBAL. These results are called input up-scaling ET. The comparisons between two aggregating approaches will reveal if the model predictions are impacted by the change in data aggregation methods. Figure 4.11 presents ET maps created by two aggregation methods, at spatial resolutions of 60m, 120m, 240m, 480m and 960m. Basic statistics are listed in Table 4.6.

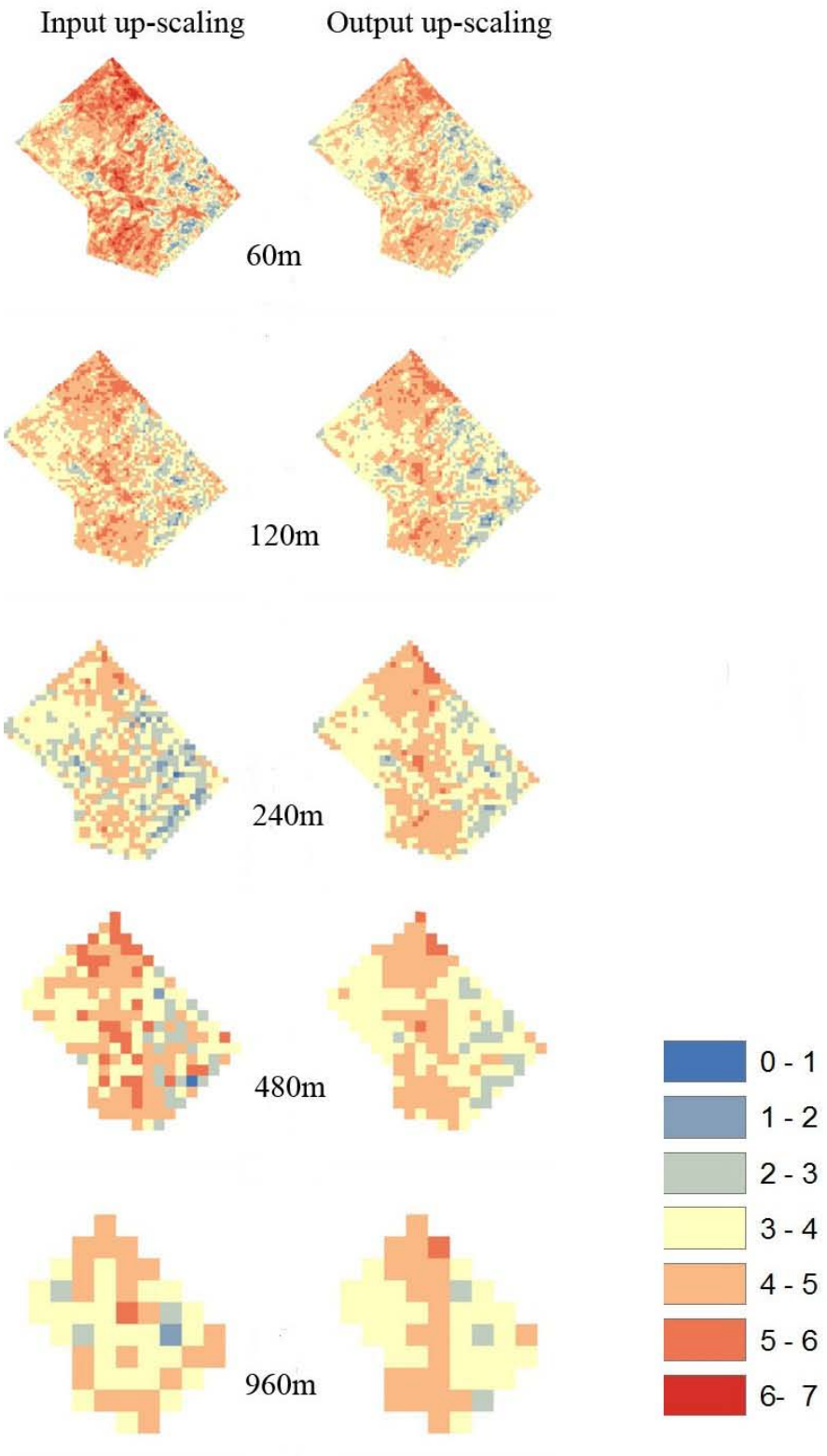

Figure 4.11 Two maps of ET at from 60m to 960m resolutions.

Table 4.6 Basic statistics of two ET maps on September 18, 2005

	Input up-scaling ET (mm/day)				
	60m	120m	240m	480m	960m
Min	0.2	0.83	0.94	0.91	1.89
Max	6.88	5.73	5.31	5.83	5.03
Mean	4.31	4.03	3.5	4.06	3.81
Std	1.03	0.77	0.8	0.86	0.68

	Output up-scaling ET (mm/day)				
	60m	120m	240m	480m	960m
Min	0.3	0.85	1.52	2.39	2.78
Max	5.89	5.67	5.51	5.12	5.11
Mean	3.87	3.87	3.86	3.84	3.88
Std	0.83	0.79	0.71	0.61	0.54

In general, input up-scaling method keeps extreme ET values while output up-scaling method has more homogenous ET distribution. The coarser the resolution, the more homogenous ET becomes for both aggregation methods. The standard deviation values of input up-scaling ET are higher than that of output up-scaling ET, except for 120m, when the latter is slightly higher than the former.

To compare if ET calculated from two methods are significantly different, paired samples t-test was conducted on 60% of pixels from each of the two ET datasets from 60m to 960m resolutions (Table 4.7). The null hypothesis is that the mean value of ET from input up-scaling equals the mean of ET from output up-scaling.

Table 4.7 Paired samples t-test of two ET datasets

Resolutions	Paired Samples Correlations			Paired Samples Test		
(m)	N	Correlation	Sig.	t	df	Sig.(2-tailed)
60	8031	0.979	0.000	139.581	8030	0.000
120	2070	0.962	0.000	34.537	2069	0.000
240	487	0.919	0.000	-25.878	486	0.000
480	138	0.797	0.000	4.015	137	0.000
960	29	0.632	0.000	-0.533	28	0.599

Two ET are highly correlated at all scales, the finer the resolution, the higher the correlation is. The signification values from 60m to 480m are 0, smaller than 0.05, thus the null hypothesis is rejected. Mean value of ET from input up-scaling is significantly different from the mean of ET from output up-scaling. However, at 960m, the significant value is bigger than 0.05, which indicates there is not a statistically significant difference between two ET datasets.

A pixel by pixel comparison of these two maps was performed to examine the differences between the two ET maps in further details (Figure 4.12). The relative difference was calculated as ET from input up-scaling minus ET from output up-scaling at corresponding resolutions to examine where the values differ and to aid in explaining why they differ. Three breaking points were chosen to divide the differences: -25%, 0, and 25%.

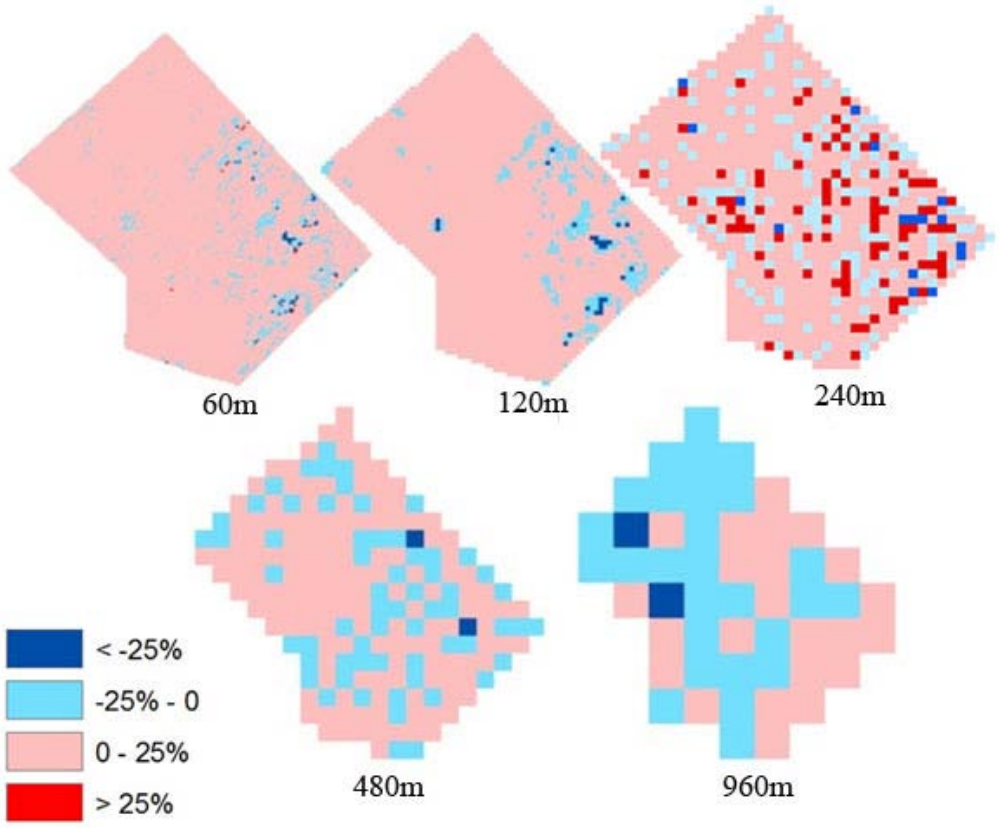

Figure 4.12 Pixel by pixel comparison across scales.

At 60m resolution, about 93% of all pixels are within 0-25% change category. The second biggest category is -25%-0, taking about 6.5%. The two biggest categories add up to 99.5%. A closer look was taken on the relative difference map with the land cover map as reference. Those pixels falling into <-25% and >25% category are mostly on the boundary of areas of different land cover classes, particularly the mixed area of grass and non-vegetated surfaces.

When the resolution is 120m, the difference map shows that most of them, about 92% of all pixels fall into the category of 0-25%. Actually, 91.6% of them are within 1% difference. The second biggest category is -25%-0, taking about 7%. The results show that at 120 meters although the resolution becomes coarser, the relative differences

between these two products are smaller, and most of them underestimate ET by 0-2%. While taking a closer look at the relative difference map, those pixels falling into <-5% category are on the boundary of areas of different land cover classes and some on the non-vegetated surfaces while ET is low.

When the resolution is 240m, the difference map displays that most of them, about 69% of all pixels fall into the category of 0-25%. The second biggest category is -25%-0, taking about 19%. When the resolution is 480m, the difference map displays that about 30% fall into the category of -25%-0, and 69% in the category of 0-25% (actually 0-3%). When the resolution is 960m, the difference map displays that 51% fall into the category of -25%-0, and 45% in the category of 0-25% (actually 0-7%).

These findings indicate that when using two aggregation techniques to estimate ET, most (between 88.0% -99.5%) of relative difference at each pixel are within ±25% from resolution at 60m to 960m. Comparing with land cover map, boundaries of mixed neighboring areas (e.g. grass and non-vegetated surfaces) and non non-vegetated surfaces are where most of bigger differences (>25% and <-25%) occur.

ET by land cover classes are further summarized to compare ET estimated using two aggregation techniques (Figure 4.13). The orders of ET from high to low are the same. However, the mean ET from input up-scaling values for all land cover classes are higher than those of mean ET from output up-scaling. The difference is highest in forest areas, followed by shrub, grass and non-vegetated areas. At 960m, no pixels are classified as non-vegetated areas.

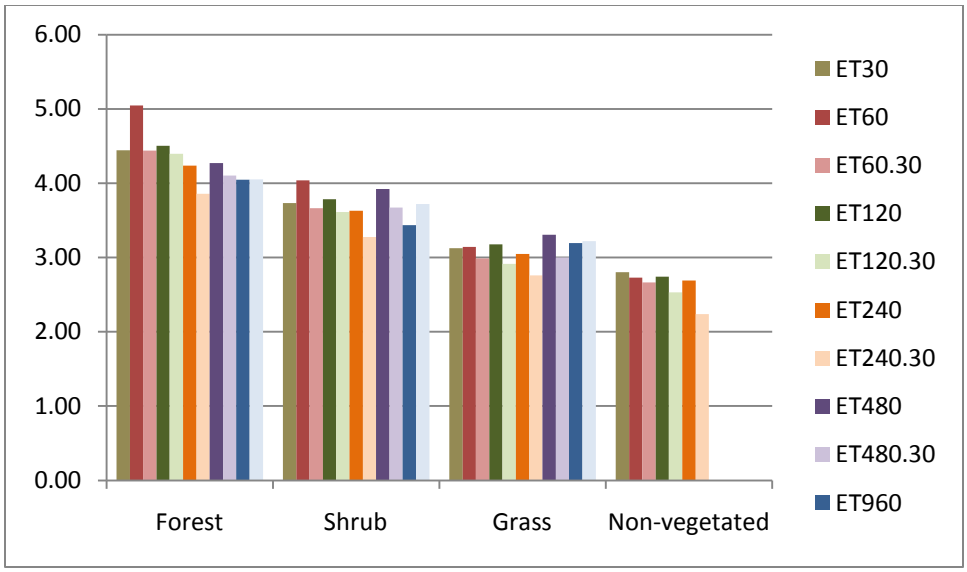

Figure 4.13 ET by land cover class across scales.

A one-way ANOVA test was performed to compare the means of ET from each land cover class at resolutions from 30m to 960m (Table 4.8). This test confirms that ET values are significantly different for each land cover class at all resolutions (i.e., all significance values are less than 0.05).

Table 4.8 One way ANOVA test of mean ET for each land cover class

	Input up-scaling		Output up-scaling	
resolution (m)	F value	Sig.	F value	Sig.
30	13672.56	0	13672.56	0
60	6014.323	0	4785.55	0
120	1064.795	0	1382.592	0
240	117.974	0	207.507	0
480	10.474	0	37.461	0
960	8.053	0.001	8.982	0

To study if aggregation techniques alter spatial patterns, three metrics have been chosen to compare two ET maps across scales including Number of Patches (NP), and Patch Ratio (PR). Table 4.9 shows the metrics of recoded ET maps across scales. At 60

meters, ET from input up-scaling has 70% more patches than that of ET from output up-scaling. When resolutions become coarser, this pattern remains. However, at 960 meters, the numbers of patches for ET from input up-scaling and ET from output up-scaling are very close. When resolutions become coarser, both PR values for ET from input up-scaling and ET from output up-scaling increase, with the PR from ET from input up-scaling always bigger than that for ET from output up-scaling. This finding indicates that the entire area is less fragmentized with increasing pixel size. When the resolution is 960m, two ET products have similar number of patches.

Table 4.9 Metrics of recoded ET

	Input up-scaling		Output up-scaling	
resolution (m)	NP	PR	NP	PR
30	678	1%	678	1%
60	686	5%	402	3%
120	230	7%	184	5%
240	83	10%	51	6%
480	37	18%	17	8%
960	10	19%	9	17%

The first research question is about the role of aggregation technique in a non-linear model for ET estimation. To evaluate the ET differences from aggregation techniques, comparisons between ET estimates using two aggregation techniques are studied from three perspectives: correlation, pixel by pixel difference, and statistics by land cover class. Findings are 1) the correlation between ET estimated by two aggregation techniques is high, and decreased with coarser resolutions 2) there is a significant difference between two ET datasets at resolutions finer than 960m 3) pixel by pixel differences are mostly within ±25% 4) ET statistics for each land cover are in the

same order and land cover dependent 5) the spatial patterns of ET are dependent on the aggregation techniques.

A non-linear process influenced by multiple factors, ET estimation contains three sources of uncertainty: choice of vegetation parameterization, surface temperature and the source of net radiation data (Ferguson et al. 2010). The study in this dissertation discovered the combined influence of multiple inputs on ET is close to linear. The finer the resolution is, the closer it is to linear. Moreover, the statistical summary for each land cover class from non-linear estimation are in the same order as from linear estimation. When the spatial resolutions become coarser, the landscape heterogeneity causes uncertainty in ET estimation. The boundaries along mixed land cover classes are where stronger non-linear impact exists. Thus, in a homogenous area, ET can be calculated using the linear aggregation from finer to coarser scales, whereas at a heterogeneous area, the non-linear impact cannot be ignored. If the study focus is about the spatial pattern of ET, the non-linear aggregation method is suggested for both homogenous and heterogeneous areas.

4.3.2 The Relationship between Evapotranspiration and its Indicators across Scales

The second research question is about the scale dependency between ET and its indicators, surface temperature and NDVI. To identify a scale dependency, linear regressions was performed on ET, based on the two aggregation methods, for NDVI and surface temperature (Figure 4.14-Figure 4.19). Their R^2 are listed in Table 4.10.

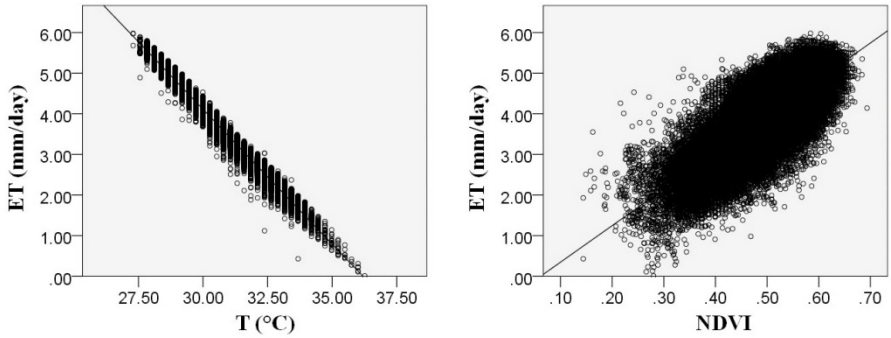

Figure 4.14 Linear regressions at 30m.

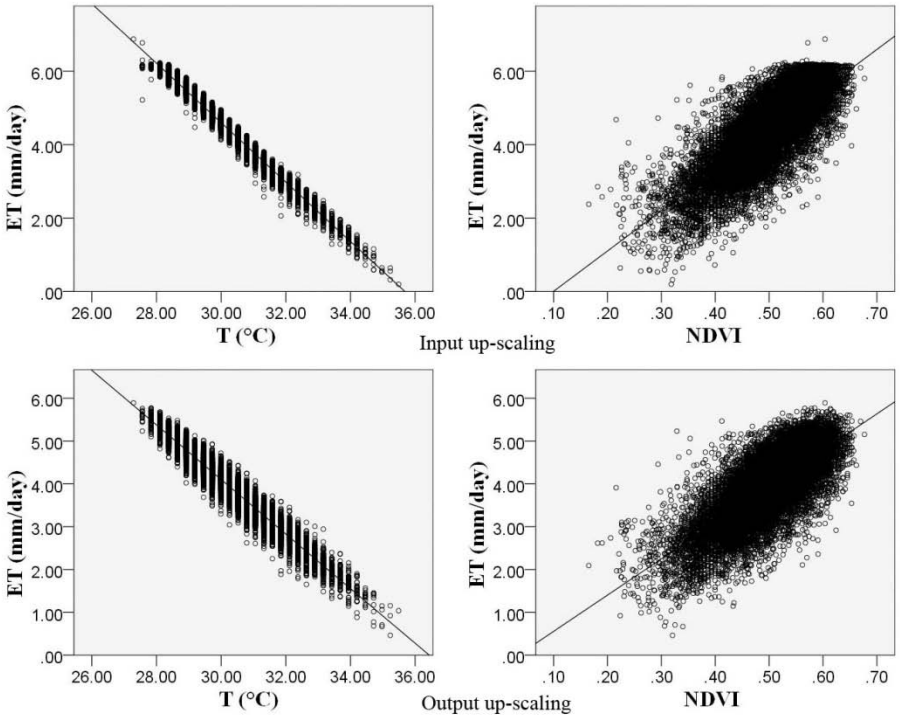

Figure 4.15 Linear regressions at 60m.

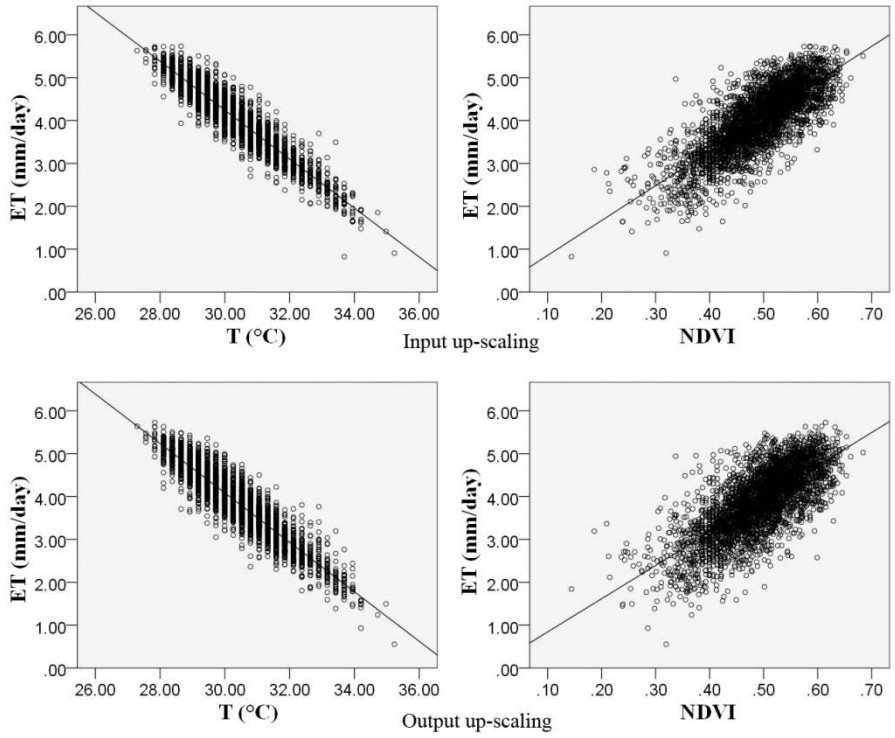

Figure 4.16 Linear regressions at 120m.

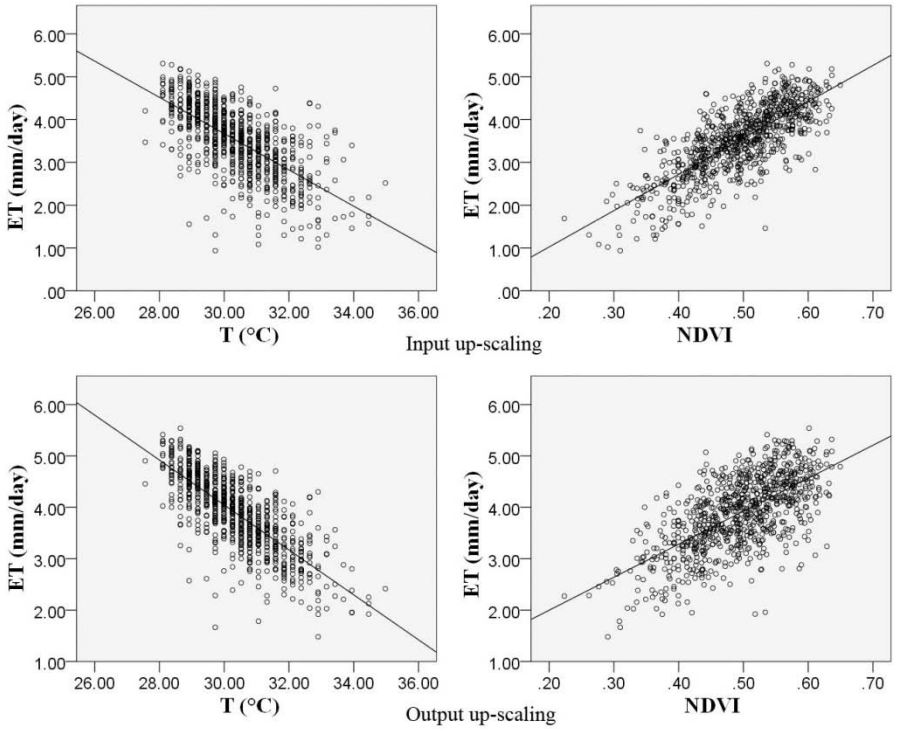

Figure 4.17 Linear regressions at 240m.

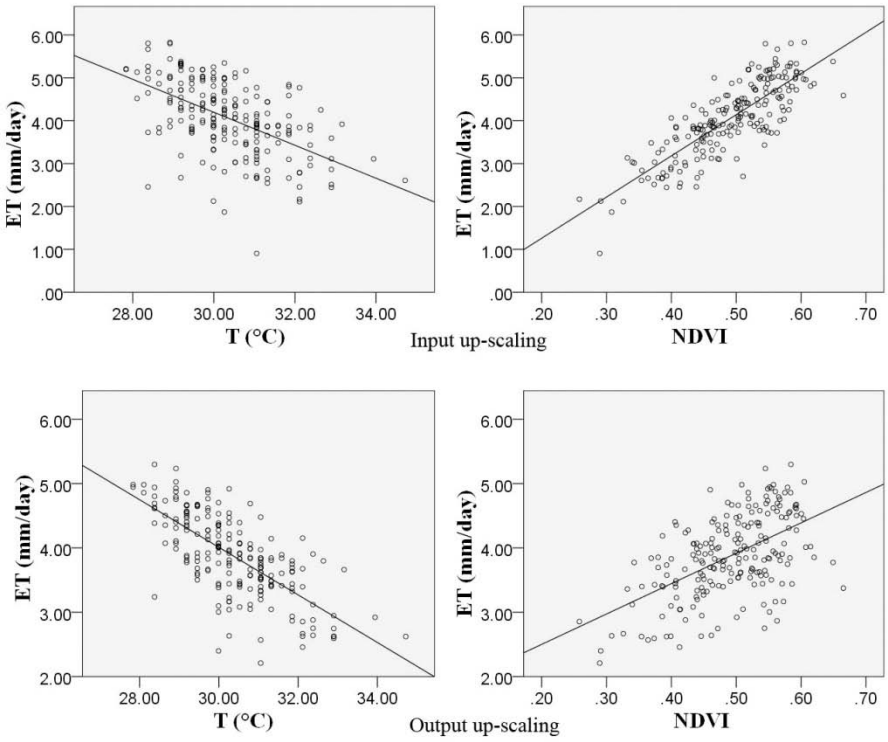

Figure 4.18 Linear regressions at 480m.

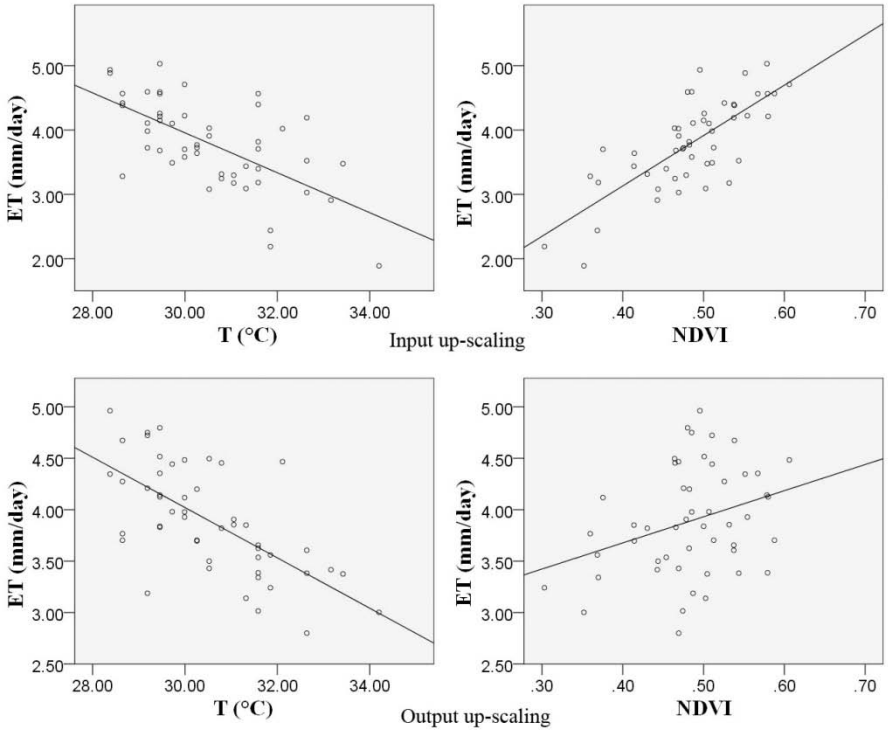

Figure 4.19 Linear regressions at 960m.

Table 4.10 R^2 for ET from output up-scaling and ET from input up-scaling

Resolution (m)	Input up-scaling		Output up-scaling	
	NDVI	T	NDVI	T
30	0.61	0.98	0.61	0.98
60	0.61	0.98	0.56	0.94
120	0.61	0.89	0.52	0.86
240	0.44	0.59	0.58	0.42
480	0.67	0.29	0.30	0.50
960	0.56	0.41	0.10	0.43

(P-value < 0.05)

The trends of R^2 (Figure 4.20) show that ET estimations from both aggregation methods have stronger correlation with surface temperature than NDVI at resolutions finer than 120m, while the correlations decrease with decreasing resolutions. At resolutions coarser than 120m, correlation patterns of the drivers of ET are inconsistent. With coarsening resolutions, individual pixels are likely to cover heterogeneous landscape. The correlations of ET with surface temperature and NDVI change with scale due to the change of landscape heterogeneity. The correlation values are dependent on aggregation methods, while at finer resolutions, the differences are smaller than those at coarser resolutions.

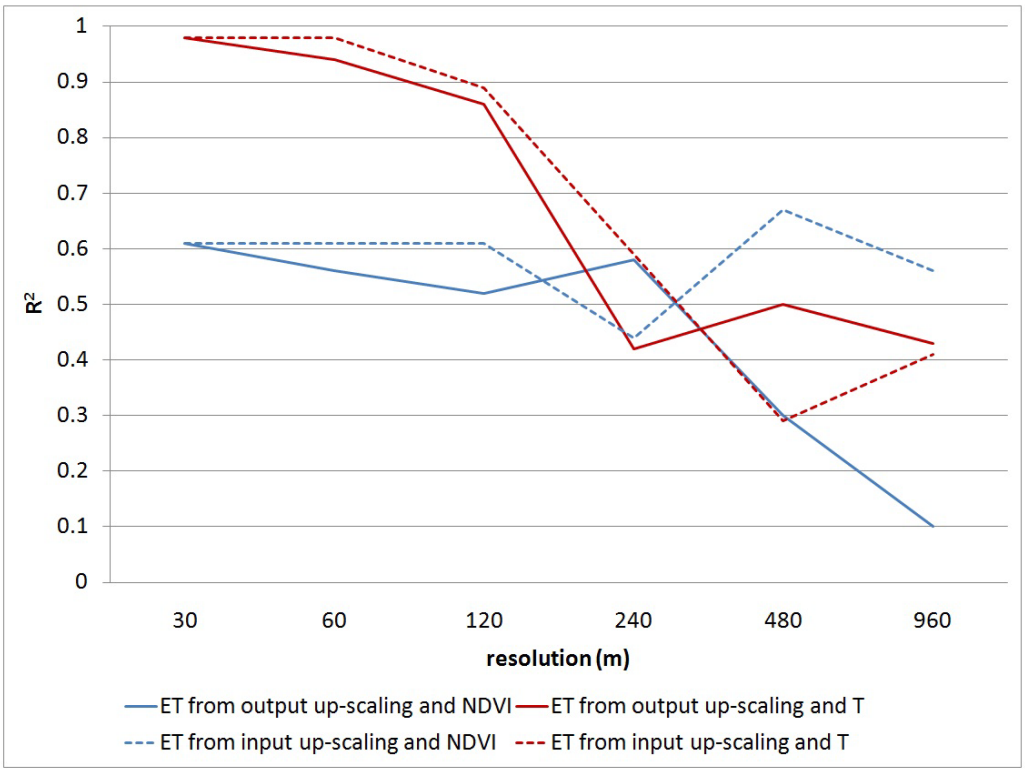

Figure 4.20 R^2 for ET, NDVI and surface temperature across scales.

4.3.3 Spatial Autocorrelation Analysis

The third research question in this dissertation focuses on the role that spatial resolution plays in the spatial pattern of ET. In this part, geostatistical analysis was performed on ET estimated at various spatial resolutions. The purpose was to identify the relationship between the spatial autocorrelation of ET and the resolution. Semivariograms were analyzed for ET on day 261 at resolutions from 30m to 960m (Figure 4.21-4.22 and Table 4.11). There are several models for fitting the semivariograms, including linear,spherical, Gaussian, exponential, and power models. In this study, all models available were tested and the models with lowest root-mean-square error were chosen to best fit the semivariograms.

When resolution was finer than 480m, ranges were approximately equal for ET from input up-scaling and ET from output up-scaling. Figure 4.22 shows that at 480m and 960m, it was difficult to identify the range for spatial autocorrelation of the study site since there is not a constant sill identifiable.

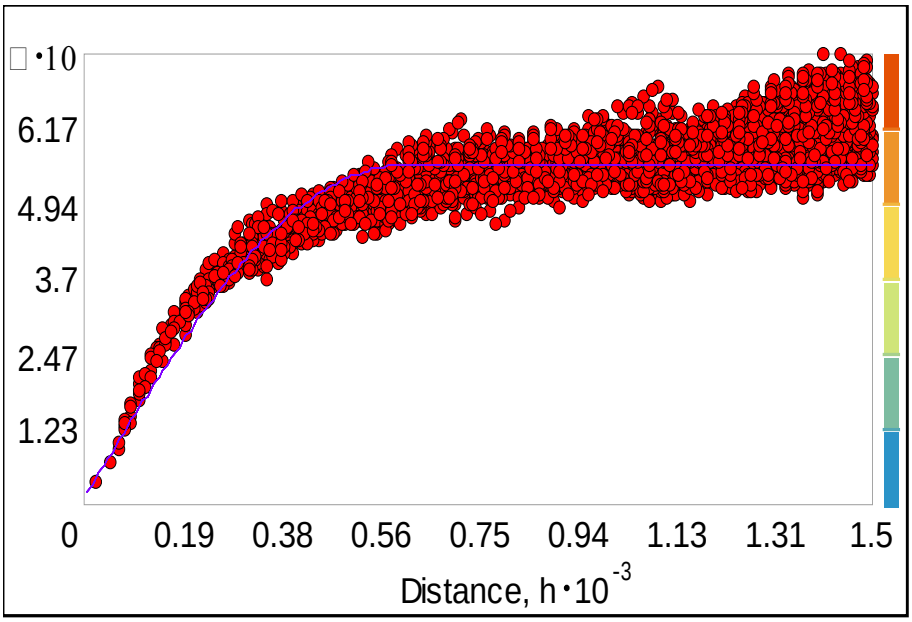

Figure 4.21 Semivariogram analysis of ET at 30m.

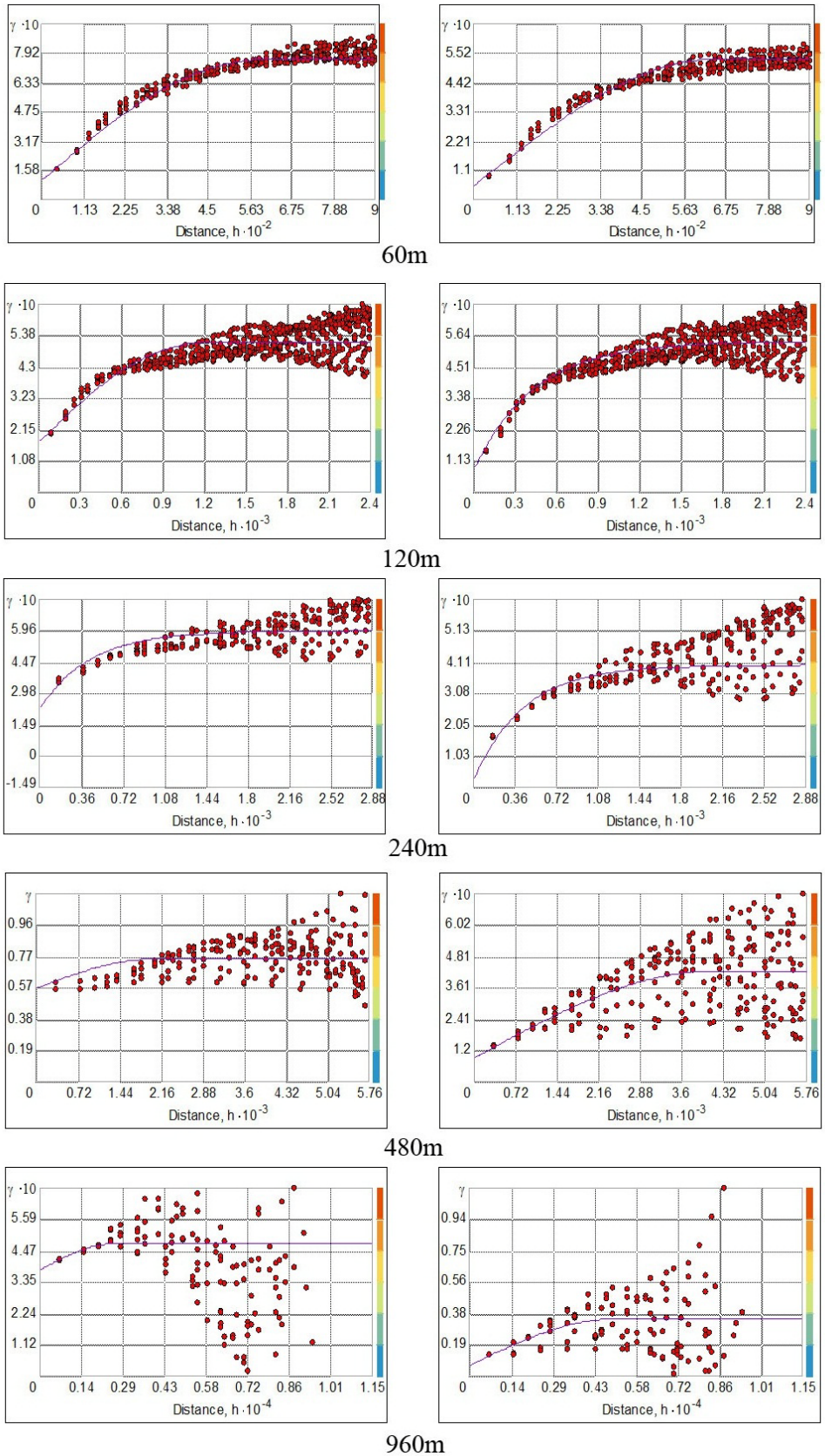

Figure 4.22 Semivariogram analysis of ET across scales from 60m to 960m.

Table 4.11 Parameters for the semivariogram analysis

	Input up-scaling			Output up-scaling		
Resolution (m)	Nugget	Partial sill	Range	Nugget	Partial sill	Range
30	0.01	0.55	650	0.01	0.55	650
60	0.10	0.66	650	0.05	0.48	650
120	0.17	0.35	1400	0.08	0.46	1300
240	0.29	0.26	1500	0.13	0.25	1500
480	0.57	N/A	N/A	0.07	N/A	N/A
960	0.35	N/A	N/A	0.09	N/A	N/A

Range represents the distance within which pixels are spatially autocorrelated, where locations beyond are not. When the resolution is finer than 480m, both ET from input up-scaling and ET from output up-scaling have obvious ranges. The variance increases with distance and becomes constant when the distance is on the order of 650-1400m. When the resolution is coarser than 240m, there is not a range identifiable for spatial autocorrelation. At 480m, the variance among closer pixels are similar to the variance among further pixels At 960m, the variance among close pixels are bigger than the variance among further pixels.

The range identified with the 30m resolution data indicates that ET beyond 650m is spatially uncorrelated. To accurately model ET, therefore, the resolution should be smaller than this range value (i.e., 650m). However, what resolution can best present the spatial variability is still unknown. The partial sill is used as an indicator, since it represents the variance of a spatially autocorrelated process without any nugget effect. The partial sill values are plotted in Figure 4.23.

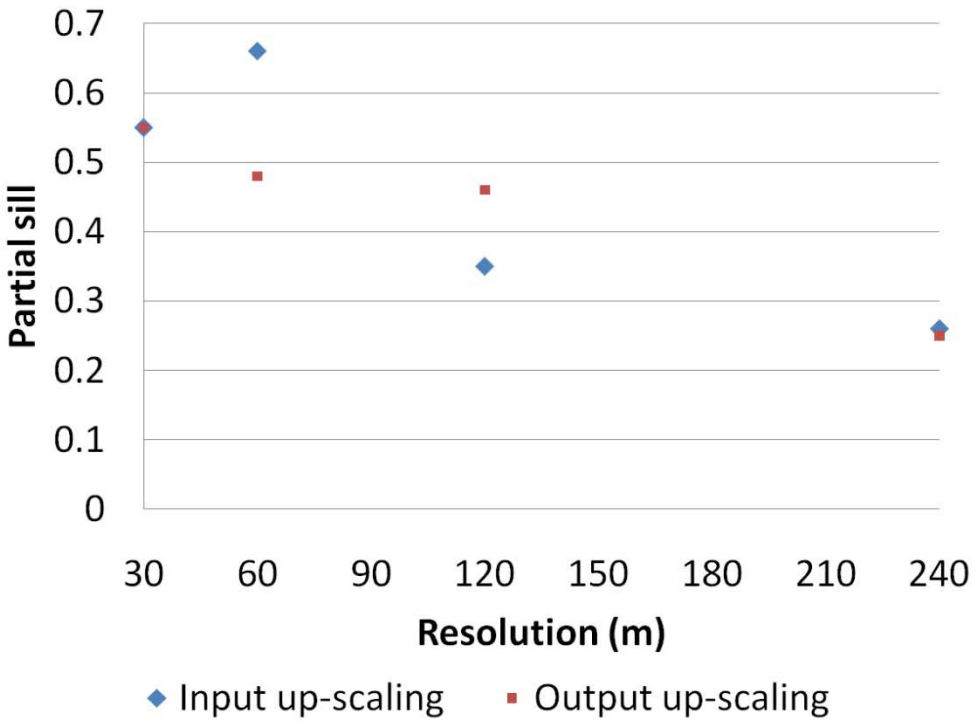

Figure 4.23 Partial sill values across scales.

In general, partial sill values are higher at finer resolutions. The maximum variance of ET from output up-scaling occurred at 30m. However, the maximum variance of ET from input up-scaling occurred at 60m. This finding reveals that the finest resolution does not necessarily best represent the spatial variability in the dataset. As stated earlier, ET is dependent on the land cover classes. To accurately represent the spatial variance of ET, the landscape heterogeneity should be considered. Some factors including patch size, patch shape and the distribution of patches can be used to quantify the landscape composition. The ideal resolution should have the highest partial sill value in the semivariogram analysis. This finding has three indications: 1) fine resolution can better present the variance of landscape than coarse resolution 2) the finest resolution

may not be the best resolution to reflect the spatial variability 3) the best resolution is impacted by the aggregation method.

The implications of findings in this subsection are the spatial resolution plays an important role in the study of spatial pattern. The selection of spatial resolution would lead to different levels of aggregation, as a result altering the spatial pattern. The value difference in neighboring pixels are close to zero at finer resolutions, and increase with coarsening resolution, then becomes smaller again due to the averaging inherent in the aggregation process. For a particular study area, a range exists when the resolution is finer than a particular threshold. At resolutions finer than a threshold (e.g. 480m in this study), the range of spatial autocorrelation is identifiable. When resolutions are coarser than the threshold, the range of spatial autocorrelation disappears. The choice of resolution not only impacts the identification of range but also the spatial variability that can be measured in the entire study area. Not simply the finest resolution is the best, partial sill should be used to evaluate if a resolution can accurately represent the spatial variability.

4.4 Discussions

The SEBAL model needs two pixels to represent very dry and very wet conditions. These two pixels serve as the extreme values in ET estimation. In this study, since there is no irrigation in the study area, the wet pixel is instead selected in forested areas that have the lowest temperatures – these will be the wettest pixels. Many low temperature, forested pixels were iteratively tested as the wet pixel to examine the impact of different wet pixels on ET estimation. Findings show that there are negligible differences in ET estimation that resulted from different wet pixels. Thus, although the

selection of wet and dry pixels is subjective, as long as the selection meets the criteria (e.g. low temperature and forest in this study), ET estimation is reliable.

Uncertainty in the eddy covariance measurements made at the three sites at Freeman Ranch presents challenges for validating remotely sensed estimates of ET. Without additional processing, the uncertainty associated with eddy covariance measurements is about 20% due to non-closure of the energy balance (Farahani et al. 2007; Twine et al. 2000; Wilson et al. 2002). The field data in this study have been processed to close the energy balance (Moore and Heilman 2011), but there is still a small mismatch between ET estimated from remotely sensed data and measurements from eddy covariance towers. Part of the difference is attributable to the timing of satellite overpass. The satellite passes over the study site at 10:55 am local time, 5 minutes before the eddy covariance towers and the weather station make measurements. Although it is only a 5 minute delay, the parameters from the weather station (e.g., wind speed and air pressure) may change during this short period, which in turn will have an impact on the ET calculated using the SEBAL model. It is expected, however, that these differences are minimal.

The footprint of an eddy covariance tower is dependent on sensor height and local surface roughness, and changes continuously as climate parameters change. Li et al. (2008) compared satellite-based surface energy balance models and tower-based flux measurements over heterogeneous landscapes and found a good agreement at the 30 m and 120 m resolutions. However, due to the influence of wind direction and local surface roughness, the footprint of a flux tower may be an irregular shape which leads to a mismatch between the actual flux tower footprint and the square shaped pixel of satellite

imagery. This means that the footprint of the flux tower and the pixel size do not match and that the difference in sizes varies over time. The differences in size could potentially contribute to greater ET estimation error when using satellite imagery. I do not, however, consider this error to be large in this case because ET values estimated by SEBAL at the pixel level are highly correlated with ET measured by the flux towers. The temporal trends of ET estimated by SEBAL also parallel those of ET measured by the flux tower.

Although SEBAL is a reliable ET estimator, some factors should to be considered to improve its estimation accuracy. In SEBAL, weather variables (i.e. wind speed, air temperature and air pressure) are assumed to be uniform across the entire study area, when in reality the effects of surface heterogeneity on weather occur at a much smaller scale (e.g., a 5-10 km area) (Wieringa 1986). In reality, there might be some variations for each parameter that could be modeled by placing more measurement instruments in the study area and then interpolating spatially varying weather surfaces.

Other biophysical factors specific to the study site should be considered to increase SEBAL accuracy. For instance, the SEBAL model overestimated ET for all nine dates at the woodland site. Literature indicates that the soil depth at the woodland site is the shallowest (0.2 m overlying fractured indurated limestone) among the three sites, while the soil depth for savanna site is about 1.6m and 0.5m at the grassland site (Moore and Heilman 2011). Water storage capacity is limited by the depth of soil, which in turn confines water available for the ET process. Moore et al. (2009) found lower latent and higher sensible heat in shallow soil systems than what would occur in deeper soil systems. Although soil depth has an impact on the ET process, the SEBAL model does not use soil depth directly as an input parameter. Results at the woodland site reveal that

without taking the soil depth into account, SEBAL seems to overestimate ET where the soil is shallow. More work is needed to study the soil depth impact on ET estimation using SEBAL. Although the SEBAL model overestimated ET for all nine dates at the woodland site, the date selected for spatial scaling analysis has the closest ET value to the flux tower measurement (i.e. 3.7 vs. 3.8 mm/day), which is within the acceptable 10% error range described by Hendrickx and Hong (2005). Further spatial analysis based on this ET estimation from SEBAL is reasonable and the conclusions are valid.

Comparisons of ET estimated from the two aggregation methods reveal that ET from input up-scaling keeps extreme values better than ET from output up-scaling. Both aggregation methods use a low pass filter that simply averages the pixel values from higher resolutions. Equal weight is given to each high resolution pixel used to calculate a coarser resolution average. Such an equal weighting scheme reduces the spatial variability of input parameters and/or ET estimates and reduces the influence of landscape heterogeneity on the ET process. The input up-scaling method, however, minimizes aggregation errors and reflects the heterogeneity of the input parameters (e.g. NDVI, surface temperature) better than the output up-scaling method and, therefore, allows for a wider range of calculated ET estimates. The output up-scaling method only aggregates ET without considering its drivers and their spatial patterns, thus reducing spatial heterogeneity in the aggregation process. Weighted, or non-linear, aggregation methods should be evaluated in future to determine their ability to maintain extreme values resulting from landscape heterogeneity.

The equation used for ET estimation in SEBAL does not change across scales – SEBAL assumes homogenous coverage for each pixel. Theoretically, therefore, the

correlation between ET and its drivers (i.e., NDVI or surface temperature) should stay the same regardless of the scale of analysis. The correlation analysis at different scales, however, shows a non-uniform relationship between ET and its drivers. This is attributable to the increase in sub-pixel landscape heterogeneity that occurs as more pixels are aggregated to coarser resolutions. For example, results indicate that from 30m to 120m resolution, surface temperature always has a higher correlation with ET than with NDVI. At resolutions coarser than 120m the relationships between ET estimation and its drivers unexpectedly switches order – NDVI has a higher correlation with ET than surface temperature. An alternative explanation of the results is that surface temperature has its greatest influence on ET at finer scales and NDVI has its greatest influence at coarser scales.

Semivariogram analysis is used to model spatial autocorrelation, and has been used to provide an estimate of the minimum resolution at which to represent land cover types (Atkinson and Lewis 2000). Kustas et al. (2004) suggested the range value indicates the resolution at which to model land cover since, they argue, the range corresponds to the land cover patch size. Resolutions greater than the range value will contain mixed land cover types. My study, however, shows that the range value consistently increases as the resolution becomes coarser. Since the size of actual land cover patches does not increase simply because the pixel resolution becomes coarser, I argue that the range value is not the best indicator of patch size. I argue, instead, that the partial sill is a better indicator of the most appropriate patch size, and is therefore indicative of the resolution at which ET should be modeled. The nugget is a measure of differences between pixel values that are immediately adjacent, and when the nugget is

large the resolution closely matches the land cover patch size. It would appear the nugget could be used to indicate the most appropriate resolution at which to model ET, except that it is not possible to compare nugget values for different aggregation techniques without being able to first standardize them. Standardization is necessary because the each dataset has different sill values (i.e., the total range of modeled semivariance). The partial sill is the difference between the total range of variance and the nugget and can be used as a standardized measure for comparing different resolutions of imagery. I argue that the resolution that produces the highest partial sill is the most appropriate resolution for modeling the spatial variability of ET.

CHAPTER V

CONCLUSION AND FUTURE WORK

This study exemplifies how remotely sensed data can provide a way to investigate the scale dependency of mass and energy fluxes in the hydrologic cycle. In this dissertation, a means was developed to analyze the scaling relationships that exist in a complex system. Factors impacting the scaling relationship include aggregation techniques, drivers or indicators of the phenomenon, and the spatial resolution used in the study. Scale changes lead to the change of spatial pattern, the correlation between input and output as well as the spatial autocorrelation. The objectives of this research were to 1) identify aggregation effects in the upscaling process, 2) examine correlations of NDVI and surface temperature with ET estimations across scales, and 3) investigate the impact of spatial resolution of remotely sensed data on the observance of the spatial autocorrelation of ET.

To answer three research questions, ET estimated from remotely sensed data in the SEBAL model were compared with ET measured by the eddy covariance technique at three tower sites at Freeman Ranch, Texas. ET was measured between March and December of 2005 at grassland, woodland, and savanna sites. R^2 values between ET from SEBAL and in-situ were 0.81 at grassland, 0.87 at savanna, and 0.76 at woodland. ET from SEBAL overestimated ET at the woodland site. Temporal comparisons also show

that ET values from LANDSAT 7 at three sites have the same trends as those from eddy towers. ET values were highest in June at all three sites. The lowest values appeared in December. The validation shows ET from SEBAL is reliable for further ET study.

Next, the temporal pattern of ET was analyzed with NDVI, surface temperature, and length of day. ET is found to highly relate to the length of day with an R^2 of 0.97, which indicates that length of day is the major temporal indicator of ET. The spatial pattern of ET was studied by comparing the patterns of surface temperature, NDVI, and land cover at resolution of 30m. Surface temperature was found to have a strongly negative relationship with ET (i.e. an R^2 of 0.98), while NDVI had a positive but less strong relationship with ET (i.e. an R^2 of 0.61). Land cover and ET have very similar spatial patterns.

In achieving the first objective, two aggregation techniques are used to aggregate ET from finest resolution (i.e. 30m) to coarser (i.e. 60m, 120m, 240m, 480m and 960m). One is to scale up ET by averaging ET calculated at 30m. The other one is to average the input data from 30m and then calculate ET in SEBAL. ET results are called ET from output up-scaling using the first approach and ET from input up-scaling using the second approach. Statistics, pixel by pixel difference and spatial patterns of two ET results were compared to see the differences created by two aggregation techniques. In general, ET from input up-scaling had a wider range than ET from output up-scaling and maintained extreme values during the aggregation process while ET from output up-scaling moderates out the extreme values. In addition to differences in minimum, maximum, mean and range values, paired sample t-tests showed that when the resolutions are finer than 960m, ET from input up-scaling is significantly different from ET from output

up-scaling. Linear regression shows that the correlation between ET from input up-scaling and ET from output up-scaling decreases with coarsening resolutions. Pixel by pixel comparison of two ET results reveals that differences vary with scales, while most of the differences are within ±25%. The spatial patterns of ET from input up-scaling and ET from output up-scaling show that although having different number of patches, both ET distributions become more homogenous when the scale is coarser. Both aggregation techniques show that ET is significantly different among different land cover classes.

The second objective of the study was to study the scale dependency of ET estimation on NDVI and surface temperature across scales. Linear regression shows that surface temperature is more correlated to ET than NDVI when resolutions are finer than 240m. Both surface temperature and NDVI have decreasing correlation with ET when the resolution decreases. When resolution is coarser than 240m, the correlations become inconsistent. The landscape heterogeneity plays a role in the relationships between ET and its external and internal indicators. The impact of heterogeneity can alter the correlation of ET and the inputs for ET estimations across scales. The correlation is also dependent on aggregation methods.

The third objective was to study the relationship between the spatial resolutions of remotely sensed data and the spatial autocorrelation of ET. Semivariogram analysis was conducted on ET across scales. Range and partial sill were used to study the spatial autocorrelation of ET. When the resolution is finer than a threshold (i.e. 480m in this study), ranges are identifiable (i.e. on the order of 650-1400m in this study). When the resolution is coarser, it becomes difficult to find a range. Finer resolution can better represent the variance of the landscape than coarse resolution. However, the finest

resolution may not be the best resolution to reflect the spatial variability. In this study, ET from output aggregation has the highest variance at 30m resolution, while ET from input up-scaling has the highest variance at 60m resolution. The resolution having the highest partial sill value can best present the landscape's spatial variability. We should be cautious to draw conclusions about no spatial autocorrelation since it is possible that the resolution is too coarse to reflect the heterogeneity of the landscape.

Although a lot of efforts have been devoted to research in scale issue, there is no general method for scaling relationship. This is partly due to a lack of understanding for processes and patterns in complex systems that are scale dependent. This research provides a way to study the scaling relationship in the following steps. First, it is essential to have a general understanding of the phenomenon and the drivers. In this particular study, ET and the major inputs for ET estimation including NDVI and surface temperature are calculated. ET is found to have the highest correlation with surface temperature. The spatial pattern of ET is dependent on the distribution of land cover classes. Next, the landscape heterogeneity should be considered. When scale changes, the landscape heterogeneity may change. As a result, the correlation between ET and its input parameters can be altered. The landscape heterogeneity also determines the spatial autocorrelation, which can be evaluated by conducting a geostatistical analysis. Finest resolution can be used to identify a range for spatial autocorrelation. However, finest resolution may not be the best one to represent the maximum spatial variability. Partial sill reveals the variance of the landscape. Resolution with highest partial sill should be the one to use for best representation of landscape variance. Third, for a non-linear

process, input up-scaling aggregation method keeps the extreme values better than output up-scaling aggregation method.

Taken as a whole, the findings indicate that input up-scaling is the best method of data aggregation because it (1) maintains extreme values, (2) produces ET estimates that are more highly correlated with its drivers, and (3) produces ET estimates with the largest partial sill value. Each of these reasons suggests that landscape heterogeneity is key to studying the scaling relationship of a non-linear biophysical process. In order to capture a biophysical process accurately, we must consider the impacts of each spatially heterogeneous input parameter. Simply aggregating estimated results from the finest resolution without taking into account each input parameter's spatial pattern leads to the loss of spatial details. Landscape heterogeneity also impacts the relationship between causes and effects when scale varies. We must be cautious when we study scale-dependent cause and effect relationships. Relationship captured at finer resolutions may not exist at coarser resolutions because of changes in landscape heterogeneity. The scale-dependency of landscape heterogeneity also determines the spatial variability of the biophysical phenomenon.

Future work can be conducted with the following topics. This study reveals that the correlations between ET and NDVI, surface temperature become inconsistent at resolutions coarser than 120m. How the heterogeneity of landscape impacts the correlations between ET and its input needs further investigation. In this study, the range for spatial autocorrelation exists only when resolutions are finer than 480m. The range values are on the order of 650-800m. The relationship between the range value and spatial resolution can be a topic for further study. Resolution bearing the maximum

variance is not the finest resolution for spatial variability representation. How the landscape heterogeneity impacts the relationship between the spatial resolution and spatial variance remains uncertain.

REFERENCES

Addiscott, T. 1993. Simulation modelling and soil behaviour. *Geoderma* 60: 15-40.

Ahmad, M., T. Magagula, D. Love, V. Kongo, M. Mul, J. Kinoti. 2005. Estimating actual evapotranspiration through remote sensing techniques to improve agricultural water management: A case study in the transboundary Olifants catchment in the Limpopo Basin, South Africa. 6th WaterNet/WARFSA/GWP Annual Symposium, 1-4 November 2005, Ezulwini, Swaziland.

Alexandridis, T., P. Cayrol, J. Moreno, I. Cherif, Y. Chemin, C. de la Vega, R. Escudero, G. Galanis, G. Tsakoumis, N. Silleos, E. Stavrinos, G. Zalidis, and P. Duthil. 2009. Agricultural Water Consumption Services for Southern European Basins. Poster presented at the 5th World Water Forum "Bridging Divides for Water", Istanbul, Turkey, March 16-22, 2009.

Allen, R., M. Tasumi, A. Morse, R. and Trezza. 2005. A Landsat-based energy balance and evapotranspiration model in Western US water rights regulation and planning. *Irrigation and Drainage Systems* 19: 251-268.

Allen, R., M. Tasumi, and R. Trezza, 2007. Satellite-Based Energy Balance for Mapping Evapotranspiration with Internalized Calibration (METRIC)--Model, *Journal of Irrigation and Drainage Engineering* 133(4): 380-394.

Anderson, M., W. Kustas, and J. Norman. 2007. Upscaling flux observations from local to continental scales using thermal remote sensing. *Agronomy journal* 99: 240-254.

Atkinson, P., and P. Lewis. 2000. Geostatistical classification for remote sensing: an introduction. *Computers and Geosciences* 26: 361-371.

Balser, T., K. McMahon, D. Bart D, D. Bronson, D. Coyle, N. Craig, M.L. Mangual, K. Forshay, S. Jones, A. Kent and A. Shade. 2006. Bridging the gap between micro – and macro-scale perspectives on the role of microbial communities in global change ecology. *Plant Soil* 289(1): 59-70.

Barnes, P., S. Liang, K. Jessup, L. Ruiseco, P. Phillips, and S. Reagan. 2000. Soils, topography and vegetation of the Freeman Ranch. *Freeman Ranch Publication Series* No. 1. Southwest Texas State University Press, San Marcos, TX, US.

Bastiaanssen, W. 1998. Regionalization of surface flux densities and moisture indicators in composite terrain – A remote sensing approach under clear skies in Mediterranean climates. Ph.D. thesis, Wageningen Agricultural University, The Netherlands, 273 pp.

Bastiaanssen, W., E. Noordman, H. Pelgrum, G. Davids, and R. Allen. 2005. SEBAL for spatially distributed ET under actual management and growing conditions. *Journal of Irrigation and Drainage Engineering* 131: 85-93.

Bastiaanssen, W., M. Menenti, M. R. Feddes, and A. Holtslag. 1998. A remote sensing surface energy balance algorithm for land (SEBAL*). International Journal of Hydrology* 212-213: 198-212.

Bian, L. 1997. Multiscale nature of spatial data in scaling up environmental models. In *Scale in Remote Sensing and GIS, D.A. Quattrochi and M. Goodchild* (Eds), pp. 13–26 (Boca Raton, FL: Lewis).

Bian, L., and S. Walsh. 1993. Scale dependencies of vegetation and topography in a mountainous environment of Montana. *Professional Geographer* 45: 1-11.

Blunier, T., and E. Brook. 2001. Timing of millennial-scale climate change in Antarctica and Greenland during the last glacial period. *Science* 291: 109-112.

Bonan, G., D. Pollard, and S. Thompson. 1993. Influence of Subgrid-Scale Heterogeneity in Leaf Area Index, Stomatal Resistance, and Soil Moisture on Grid-Scale Land–Atmosphere Interactions. *Journal of Climate* 6: 1882-1897.

Brown, K., and N. Rosenberg. 1973. A resistance model to predict evapotranspiration and its application to a sugar beet field. *Agronomy Journal* 65: 341-347.

Brunsell, N., J. Ham, and C. Owensby. 2008. Assessing the multi-resolution information content of remotely sensed variables and elevation for evapotranspiration in a tall-grass prairie environment. *Remote Sensing of Environment* 112: 2977-2987.

Brunsell, N., and R. Gillies. 2003. Length Scale Analysis of Surface Energy Fluxes Derived from Remote Sensing. *Journal of Hydrometeorology* 4: 1212-1219.

Brunsell, N., R. Gillies, B. Lapenta, and S. Dembeck. 2003. Aggregation of remotely sensed vegetation and derived latent heat flux. 83rd AMS Annual Meeting, 9-13 February, Long Beach, CA.

Carmel, Y. 2004. "Aggregation as a means of increasing thematic map accuracy." In: GeoDynamics: Modelling Spatial Change and Process. P. M. Atkinson, G. M. Foody, S. E. Darby and F. Wu, Eds. Boca Raton, FL, CRC Press, 440 pp.

Carmel, Y., D. Dean, and Flather, C. 2001. Combining location and classification error sources for estimating multi-temporal database accuracy. *Photogrammetric Engineering and Remote Sensing* 67: 865-872.

Carson, D. 2000. Soil of the Freeman Ranch, Hays County, Texas. Freeman Ranch Publication Series No. 4-2000. San Marcos, TX: Southwest Texas State University Press.

Carlson, T., W. Capehart, and R. Gillies, R. 1995. A new look at the simplified method for remote sensing of daily evapotranspiration. *Remote Sensing of Environment* 54: 161-167.

Chander, G., B. Markham, and D. Helder. 2009. Summary of current radiometric calibration coefficients for Landsat MSS, TM, ETM+, and EO-1 ALI sensors. *Remote Sensing of Environment* 113: 893-903.

Cressie, N. 1991. *Statistics for Spatial Data*. Wiley, New York.

Courault, D., B. Seguin, and A. Olioso. 2005. Review on estimation of evapotranspiration from remote sensing data: From empirical to numerical modeling approaches. *Irrigation and Drainage Systems* 19: 223-249.

Curran, P. 1988. The semivariogram in remote sensing: an introduction. *Remote Sensing of Environment* 24: 493-507.

Dixon, R. 2000. Climatology of the Freeman Ranch, Hays County, TEXAS. Freeman Ranch Publication Series No. 3. Southwest Texas Staate University Press, San Marcos, TX, US.

Easterling, W., and C. Polsky. 2004. Crossing the complex divide: linking scales for understanding coupled human–environment systems. In *Scale and Geographic Inquiry, R.B. McMaster and E. Sheppard* (Eds), pp. 55-64 (Oxford: Blackwell).

Evans, T., E. Ostrom, and C. Gibson. 2003. Scaling issues in the social sciences. In *Scaling in Integrated Assessment*, J. Rotmans and D.S. Rothman (Eds), pp. 75-106 (Exton, PA: Swets and Zeitlinger).

Farah, H., W. Bastiaanssen, and R. Feddes. 2004. Evaluation of the temporal variability of the evaporative fraction in a tropical watershed. *International Journal of Applied Earth Observation and Geoinformation* 5: 129-140.

Ferguson, C., J. Sheffield, E. Wood, and H. Gao. 2010. Quantifying uncertainty in a remote sensing-based estimate of evapotranspiration over continental USA, *International Journal of Remote Sensing* 31(14): 3821-3865.

Foley, J., M. Costa, C. Delire, Ramankutty, N. and Snyder, P. 2003. Green surprise? How terrestrial ecosystems could affect earth's climate. *Frontiers in Ecology and the Environment* 1: 38-44.

French, A., T. Schmugge, and W. Kustas. 2002. Estimating evapotranspiration over El Reno Oklahoma with ASTER imagery. *Agriculture and Environment* 22: 105-106.

Gehlke, C., and K. Biehl. 1934. Certain Effects of Grouping upon Size of the Correlation Coefficient in Census Tract Material. *Journal of the American Statistical Association Supplement* 29: 663-664.

Gentine, P., D. Entekhabi, A. Chehbouni, G. Boulet, and B. Duchemin. 2007. Analysis of evaporative fraction diurnal behavior. *Agricultural and Forest Meteorology* 143: 13-29.

Gibson, C., E. Ostrom, and T. Ahn. 2000. The concept of scale and the human dimensions of global change: a survey. *Ecological Economics* 32: 217-239.

Goulden, M., J. Munger, S. Fan, B. B. Daube, and S. Wofsy. 1996. Carbon dioxide exchange by a temperate deciduous forest: response to interann4al changes in climate. *Science* 271: 1576-1578.

Goward, S. , J. Tucker and D. Dye. 1985. North American vegetation patterns observed with the NOAA-7 advanced very high resolution radiometer. *Vegetatio* 64: 3-14.

Gowda, P., J. Chavez, P. Colaizzi, S. Evett, T. Howell, and J. Tolk. 2008. ET mapping for agricultural water management: present status and challenges. *Irrigation Science* 26: 223-237.

Hay, G., K. Niemann, and D. Goodenough. 1997. Spatial thresholds, image-objects, and upscaling: a multiscale evaluation. *Remote Sensing of Environment* 62: 1-19.

Hendrickx, J., and S. Hong. 2005. Mapping sensible and latent heat fluxes in arid areas using optical imagery. *Proceedings of International Society for Optical Engineering*, SPIE 5811: 138-146.

Herod, A., and M. Wright. 2003. Placing scale. In *Geographies of Power: Placing Scale*, A. Herod and M. Wright (Eds), pp. 17–24 (Oxford: Blackwell).

Heuvelink, G., and E. Pebesma. 1999. Spatial aggregation and soil process modeling. *Geoderma* 89: 47-65.

Hong, S. 2008. Mapping regional distributions of energy balance components using optical remotely sensed imagery. PhD. Dissertation. Dept. of Earth & Environmental Science (Hydrology Program), New Mexico Institute of Mining and Technology, Socorro, NM, USA.

Hong, S., J. Hendrickx, and B. Borchers. 2009. Up-scaling of SEBAL derived evapotranspiration maps from Landsat (30 m) to MODIS (250 m) scale. *Journal of Hydrology* 370: 122-138.

Hughes, D. 2004. Incorporating ground water recharge and discharge functions into an existing monthly rainfall-runoff model. *Hydrological Sciences Journal* 49(2): 297-311.

Irish, R. 2000. Landsat 7 science data user's handbook, Report 430-15-01-003-0. National Aeronautics and Space Administration.

Jarvis, P. 1995. Scaling: processes and problems. *Plant, Cell and Environment* 18:1079-1089.

Kite, G., and P. Droogers. 2000. Comparing evapotranspiration estimates from satellites, hydrological models and field data. *Journal of Hydrology* 229(1-2): 3-18.

Kustas, W., C. Daughtry, and P. van Oevelen. 1993. Analytical treatment of the relationships between soil heat flux/net radiation ratio and vegetation indices. *Remote Sensing of Environment* 46: 319-330.

Kustas, W., and J. Norman. 1996. Use of remote sensing for evapotranspiration monitoring over land surfaces. *Hydrological Science Journal* 41: 495-516.

Kustas, W., and J. Norman. 2000. Evaluating the effects of subpixel heterogeneity on pixel average fluxes. *Remote Sensing of Environment* 74: 327-342.

Kustas, W., F. Li, T. Jackson, J. Prueger, J. MacPherson, and M. Wholde. 2004. Effects of remote sensing pixel resolution on modeled energy flux variability of croplands in Iowa. *Remote Sensing of Environment* 92: 525-547.

Kustas, W., J. Norman, M. Anderson, and A. French. 2003. Estimating subpixel surface temperatures and energy fluxes from the vegetation index –radiometric temperature relationship. *Remote Sensing of Environment* 85: 429-440.

Kustas, W., E. Perry, P. Doraiswamy, and M. Moran. 1994. Using satellite remote sensing to extrapolate ecapotranspiration estimates in time and space over a semiarid rangeland basin. *Remote Sensing of Environment* 49: 275-286.

Lagouarde, J., F. Jacob, X. Gu, A. Olioso, J. Bonnefond, Y. Kerr, K. Mcaneney, and M. Irvine. 2002. Spazialization of sensible heat flux over a heterogeneous landscape. *Agronomie* 22: 627-633.

Lenz, J., and L. Baise. 2007. Spatial variability of liquefaction potential in regional mapping using CPT and SPT data. *Soil Dynamics and Earthquake Engineering* 27: 690-702.

Levesque, J., and D. King. 1999. Airborne digital camera image semivariance for evaluation of forest structural damage at an acid mine site. *Remote Sensing of Environment* 68: 112-124.

Levitt, P. 1998. Local-level global religion: The case of U.S.-Dominican migration. *Journal for the Scientific Study of Religion* 37:74-89.

Li, J., and S. Islam. 1999. On the estimation of soil moisture profile and surface fluxes partitioning from sequential assimilation of surface layer soil moisture. *Journal of Hydrology* 220: 86-103.

Li, F., W. Kustas, M. Anderson, J. Prueger, and R. Scott. 2008. Effect of remote sensing spatial resolution on interpreting tower-based flux observations. *Remote Sensing of Environment* 112: 337-349.

Lightowlers, C., T. Nelson, E. Setton, and C. Keller. 2008. Determining the spatial scale for analysing mobile measurements of air pollution. *Atmospheric Environment* 42: 5933-5937.

Limb, R., S. Fuhlendorf, and D. Townsend. 2009. Heterogeneity of thermal extremes: driven by disturbance or inherent in the landscape. *Environmental Management* 43:100-106.

Maayar, M., and J. Chen. 2006. Spatial scaling of evapotranspiration as affected by heterogeneities in vegetation, topography, and soil texture. *Remote Sensing of Environment* 102: 33–51.

McCabe, M., and E. Wood. 2006. Scale influences on the remote estimation of evapotranspiration using multiple satellite sensors. *Remote Sensing of Environment* 105(4): 271-285.

McDaniels, T., H. Dowlatabadi, S. Stevens. 2005. Multiple scales and regulatory gaps in environmental changes: the case of salmon aquaculture. *Global Environmental Change* 15: 9-25.

McGarigal, K., S. Cushman, and E. Ene. 2012. FRAGSTATS(4.x): Spatial Pattern Analysis Program for Categorical and Continuous Maps. Computer software program produced by the authors at the University of Massachusetts, Amherst. Available at the following web site: http://www.umass.edu/landeco/research/fragstats/fragstats.html

Mecikalski, J., G. Diak, M. Anderson, and J. Norman. 1999. Estimating fluxes on continental scales using remotely-sensed data in an atmospheric-land exchange model. *Journal of Applied Meteorology and Climatology* 38: 1352-69.

Meentemeyer, V., and E. Box. 1987. Scale effects in landscape studies. In: Turner M.G. ed., *Landscape Heterogeneity and Disturbance*. pp. 15-34. Springer-Verlag, New York, New York, USA.

Miller, J., J. Franklin, and R. Aspinall. 2007. Incorporating spatial dependence in predictive vegetation models. *Ecological Modeling* 202: 225-242.

Moore, G., and J. Heilman. 2011. Proposed principles governing how vegetation changes affect transpiration. *Ecohydrology* 4: 351-358.

Moran, M., A. Rahman, J. Washburne, D. Goodrich, M. Weltz, and W. Kustas. 1996. Combining the Penman-Monteith equation with measurements of surface temperature and reflectance to estimate evaporation rates of semiarid grassland. *Agricultural and Forest Meteorology* 80: 87-109.

Moran, S., K. Humes, and P. Pinter. 1997. The scaling characteristics of remotely-sensed variablesfor sparsely-vegetated heterogeneous landscapes. *Journal of Hydrology* 190: 337-362.

Morse, A., M. Tasumi, R. Allen, and W. Kramber. 2000. Final Report. Application of the SEBAL Methodology for Estimating Consumptive Use of Water and Streamflow Depletion in the Bear River Basin of Idaho through Remote Sensing. Idaho Department of Water Resources, University of Idaho, Department of Biological and Agricultural Engineering.

National Research Council. 2007. Analysis of Global Change Assessments: Lessons Learned. The National Academies Press. Washington, D.C.

Nelson, A., T. Oberthur, and S. Cook. 2007. Multi-scale correlations between topography and vegetation in a hillside catchment of Honduras. *International Journal of Geographical Information Science* 21: 145-174.

Nishida, K., R. Nemani, J. Glassy, and S. Running. 2003. Development of an evapotranspiration index from aqua/MODIS for monitoring surface moisture status. *IEEE Transactions on Geoscience and Remote Sensing* 41: 493-501.

Norman, J., K. Kustas, and K. Humes, K. 1995. Source approach for estimating soil and vegetation energy fluxes in observations of directional radiometric surface temperature. *Agricultural and Forest Meteorology* 77: 263-293.

O'Neill, R., C. Hunsaker, S. Timmins, B. Timmins, K. Jackson, K. Jones, K. Riitters, and J. Wickham. 1996. Scale problems in reporting landscape pattern at the regional scale. *Landscape Ecology* 11: 169-180.

Openshaw, S. 1984. *The Modifiable Areal Unit Problem*. Geobooks, Norwich, England.

Turner, M., R. Gardner, and R. O'Neill. 2001. *Landscape Ecology in Theory and Practice: Pattern and Process.* Springer-Verlag, New York, New York, USA.

Turner, B., R. Kasperson, W. Meyer, K. Dow, D. Golding, J. Kasperson, R. Mitchell, and S. Ratick. 1990. Two types of global environmental change: definitional and spatial-scale issues in their human dimensions. *Global Environmental Change* 1: 14-22.

O'Sullivan, D., and D. Unwin. 2002. *Geographic Information Analysis*. John Wiley and Sons, Inc.

Price, J. 1990. Using spatial context in satellite data to infer regional scale evapotranspiration. *IEEE Transactions on Geoscience and Remote Sensing* 28(5): 940-948.

Roy, D., J. Ju, K. Kline, P. Scaramuzza, V. Kovalskyy, M. Hansen, T. Loveland, E. Vermote, and C. Zhang. 2010. Web-enabled Landsat data (WELD): Landsat ETM+ composited mosaics of the conterminous United States. *Remote Sensing of Environment* 114(1): 35-49.

Sanchez, J., V. Caselles, and W. Kustas. 2008. Estimating surface energy fluxes using a micro-meteorological model and satellite images. *Tethys* 5: 25-36.

Sandholt, I., K. Rasmussen, and J. Andersen. 2002. A simple interpretation of the surface temperature/vegetation index space for assessment of surface moisture status. *Remote Sensing of Environment* 79: 213-224.

Santos, R., M. Oliveira, A. Escobar, R. Santos, and C. Coimbra. 2008. Spatial heterogeneity of malaria in Indian reserves of Southwestern Amazonia, Brazil. *International Journal of Health Geographics* 7(1):55.

Schmid, H. 2002. Footprint modelling for vegetation atmosphere exchange studies: a review and perspective. *Agriculture Forest Meteorology* 113:159-184.

Seguin, B., J. Lagouarde, and M. Saranc. 1991. The assessment of regional crop water conditions from meteorological satellite thermal infrared data. *Remote Sensing of Environment* 35: 141- 148.

Small, C. 2004. The Landsat ETM+ spectral mixing space. *Remote Sensing of Environment* 93: 1-17.

Snow, J. 1855. *On the Mode of Communication of Cholera*. Churchill, London. Reprinted by Hafner, New York, 1965.

Solecki,W. 2001. The role of global-to-local linkages in land use/land cover change in South Florida. *Ecological Economics* 37: 339-356.

Su, Z. 2002. The Surface Energy Balance System (SEBS) for estimation of turbulent heat fluxes. *Hydrology and Earth System Sciences* 6: 85-99.

Sun G., P. Caldwell, A. Noormets, S. McNulty, E. Cohen, M. Moore, J. Domec, E. Treasure, Q. Mu, J. Xiao, J. Ranjeet, and J. Chen. 2011. Upscaling key ecosystem functions across the conterminous United States by a water-centric ecosystem model. *Journal of Geophysical Research* 116:1-16.

Tang, Q., H. Gao, P. Yeh, T. Oki, F. Su and D. Lettenmaier. 2010. Dynamics of terrestrial water storage change from satellite and surface observations and modeling. *Journal of Hydrometeorology* 11: 156-170.

Tasumi, M., and R. Allen. 2007. Satellite-based ET mapping to assess variation in ET with timing of crop development. *Agricultural Water Management* 88: 54-62.

Tasumi, M., R. Trezza, R. Allen, and J. Wright. 2005. Operational aspects of satellite-based energy balance models for irrigated crops in the semi-arid US. *Irrigation and Drainage Systems* 19: 355-376.

Van Rompaey, A., G. Govers, and M. Baudet. 1999. A strategy for controlling error of distributed environmental models by aggregation. *International Journal of Geographical Information Science* 13(6): 577-590.

Verhoef, W., and H. Bach. 2003. Remote sensing data assimilation using coupled radiative transfer models. *Physics and Chemistry of the Earth* 28: 3-13.

Verstraeten, W., F. Veroustraete, and J. Feyen. 2008. Assessment of evapotranspiration and soil moisture content across different scales of observation. *Sensors* 8: 70-117.

Walsh, S., T. Evans, W. Welsh, B. Eentwisle, and R. Rindfuss. 1999. Scale dependent relationships between population and environment in northeastern Thailand. *Photogrammetric Engineering and Remote Sensing* 65: 97-105.

Warren, B., T. Spies, and G. Bradshaw. 1990. Semivariograms of digital imagery for analysis of conifer canopy structure. *Remote Sensing of Environment* 34: 167-178.

Wear, D., and J. Greis. 2002. The southern forest resource assessment summary report. In: Southern Forest Resource Assessment. *General Technical Report*. SRS-53. (eds Wear DN, Greis JG), US Department of Agriculture, Forest Service, Southern Research Station, Asheville, NC.

Wilbanks, T. 2006. How scale matters: some concepts and findings. Pages 21-35 in W. V. Reid, F. Berkes, T. J. Wilbanks, and D. Capistrano, editors. *Bridging scales and knowledge systems: concepts and applications in ecosystem assessment.Island* Press, Washington, D.C., USA.

Woodcock, C., A. Strahler, and D. Jupp. 1988. The use of variograms in remote sensing: I. Scene models and simulated images. *Remote Sensing of Environment* 25: 323–348.

Wu, J. 2004. Effects of changing scale on landscape pattern analysis: scaling relations. *Landscape Ecology* 19: 125-138.

Yang, D., H. Chen, and H. Lei. 2010. Estimation of evapotranspiration using a remote sensing model over agriculture land in the North China Plain. *International Journal of Remote Sensing* 31(14): 3783-3798.

Zwart, S., and W. Bastiaanssen. 2007. SEBAL for detecting spatial variation of water productivity and scope for improvement in eight irrigated wheat systems. *Agricultural Water Management* 89: 287-296.

VITA

Jiao Wang was born in Fushun, China, on October 30, 1981, the daughter of Chunai Wang and Yongshan Wang. After completing her work in work in Fushun number 2 High School, Fushun, Liaoning, China, in 1999, she entered Northwest University, Xian, China. She received the degree of Bachelor of Science from Northwest University in 2003. Then, she entered the Institute of Remote Sensing Application, Chinese Academy of Sciences and obtained the degree of Master of Science in 2006. In August 2006, she entered the Graduate College of Texas State University-San Marcos to pursue a doctoral degree in Geographic Information Science at the Department of Geography.

Email: jiaowang2012@gmail.com

This dissertation was typed by Jiao Wang.